AGU PUBLICATIONS

Water Resources Research

RESEARCH ARTICLE

10.1002/2014WR016595

Key Points:
- A new DWPS approach based on deviations between wavelet power spectra
- Unraveling novel features of flow regime alterations at intermediate time scales
- Segregating effects on overall flow regime alterations using subflow GDWPS

Correspondence to:
F.-C. Wu,
fcwu@ntu.edu.tw

Citation:
Wu, F.-C., C.-F. Chang, and J.-T. Shiau (2015), Assessment of flow regime alterations over a spectrum of temporal scales using wavelet-based approaches, *Water Resour. Res.*, *51*, 3317–3338, doi:10.1002/2014WR016595.

Received 23 OCT 2014
Accepted 7 APR 2015
Accepted article online 14 APR 2015
Published online 8 MAY 2015

Assessment of flow regime alterations over a spectrum of temporal scales using wavelet-based approaches

Fu-Chun Wu[1], Ching-Fu Chang[2], and Jenq-Tzong Shiau[3]

[1]Department of Bioenvironmental Systems Engineering, Hydrotech Research Institute and Center for Ecological Engineering, National Taiwan University, Taipei, Taiwan, [2]Department of Bioenvironmental Systems Engineering, National Taiwan University, Taipei, Taiwan, [3]Department of Hydraulic and Ocean Engineering, National Cheng Kung University, Tainan, Taiwan

Abstract The full range of natural flow regime is essential for sustaining the riverine ecosystems and biodiversity, yet there are still limited tools available for assessment of flow regime alterations over a spectrum of temporal scales. Wavelet analysis has proven useful for detecting hydrologic alterations at multiple scales via the wavelet power spectrum (WPS) series. The existing approach based on the global WPS (GWPS) ratio tends to be dominated by the rare high-power flows so that alterations of the more frequent low-power flows are often underrepresented. We devise a new approach based on individual deviations between WPS (DWPS) that are root-mean-squared to yield the global DWPS (GDWPS). We test these two approaches on the three reaches of the Feitsui Reservoir system (Taiwan) that are subjected to different classes of anthropogenic interventions. The GDWPS reveal unique features that are not detected with the GWPS ratios. We also segregate the effects of individual subflow components on the overall flow regime alterations using the subflow GDWPS. The results show that the daily hydropeaking waves below the reservoir not only intensified the flow oscillations at daily scale but most significantly eliminated subweekly flow variability. Alterations of flow regime were most severe below the diversion weir, where the residual hydropeaking resulted in a maximum impact at daily scale while the postdiversion null flows led to large hydrologic alterations over submonthly scales. The smallest impacts below the confluence reveal that the hydrologic alterations at scales longer than 2 days were substantially mitigated with the joining of the unregulated tributary flows, whereas the daily-scale hydrologic alteration was retained because of the hydropeaking inherited from the reservoir releases. The proposed DWPS approach unravels for the first time the details of flow regime alterations at these intermediate scales that are overridden by the low-frequency high-power flows when the long-term averaged GWPS are used.

1. Introduction

The last two decades have seen a paradigm shift toward a holistic approach for river management, which has led to a wide acceptance of the natural flow regime [*Poff et al*., 1997] as a reference condition for assessment of hydrologic alterations or a template for establishing environmental flow targets [e.g., *Instream Flow Council*, 2004; *Shiau and Wu*, 2004a, 2004b; *Harman and Stewardson*, 2005; *Shiau and Wu*, 2006; *Suen and Eheart*, 2006; *National Research Council (NRC)*, 2007; *Shiau and Wu*, 2007a, 2007b; *Mathews and Richter*, 2007; *Vogel et al*., 2007; *Hughes and Mallory*, 2008; *Shiau and Wu*, 2008, 2009; *Poff*, 2009; *Shiau and Wu*, 2010; *Yin et al*., 2011; *Arthington*, 2012; *Shiau and Wu*, 2013; *Acreman et al*., 2014; *Jones*, 2014]. The concept of natural flow regime assumes that the natural variations in flow magnitude, frequency, duration, timing, and rate of change are essential for sustaining riverine ecosystems and biodiversity. To characterize the natural and human-impacted flow regimes, numerous systems of hydrologic index have been developed (see extensive reviews by *Olden and Poff* [2003] and *Gao et al*. [2009]). These hydrologic indices are mainly used to assess flow regime alterations or evaluate environmental flow designs.

One of the most widely used systems is the Indicators of Hydrologic Alteration (IHA) [*The Nature Conservancy*, 2009], which were introduced in the context of the Range of Variability Approach (RVA) [*Richter et al*., 1996, 1997]. The IHA contain 33 ecologically relevant hydrologic parameters, which are categorized into five groups that characterize the magnitude of monthly flows, magnitude, duration and timing of annual extreme flows, frequency and duration of high and low pulses, and rate and frequency of flow changes. The

IHA are essentially a suite of annual statistics based on the long-term daily flow records, thus, they are unable to describe subdaily flow variations or temporal patterns other than monthly flow hydrographs. Subdaily flow variations are particularly significant at river reaches affected by hydropeaking reservoir operations, where large fluctuations typically prevail at subdaily to daily scales [*Zimmerman et al*., 2010; *Meile et al*., 2011; *Bevelhimer et al*., 2015].

To overcome the limitations of the IHA, *Shiau and Wu* [2013] employed five hydrologic parameters, viz., the Richards-Baker flashiness (RBF) index, daily hydrograph dissimilarity index, monthly flow deviation index, annual 7 days minimum flow, and 5 year flood, to assess the flow regime alterations at subdaily, daily, seasonal, annual, and interannual scales, respectively, where the RBF index is defined as the path length of flow oscillations (=sum of the absolute hour-to-hour changes in flow) divided by the sum of hourly flows over each 24 h period [*Baker et al*., 2004]. Although covering a wider range of temporal scales than the IHA, these hydrologic parameters still failed to depict the full spectrum of flow regime alterations. Moreover, the selected five scales were somewhat arbitrary because the most severely impacted temporal scales were not known a priori. Ideally, it would require an infinite number of parameters to evaluate comprehensively the flow regime alterations at all possible scales, which seems impractical if not impossible.

Wavelet analysis (WA) offers a powerful tool for detecting hydrologic alterations at multiple temporal scales simultaneously, and has been increasingly used in recent years to examine the variability in hydrological time series [*Nakken*, 1999; *White et al*., 2005; *Steel and Lange*, 2007; *Zolezzi et al*., 2009, 2011; *Shiau and Huang*, 2014]. In general, WA is a mathematical technique used to extract the dominant modes (or scales) of variability from statistically nonstationary time series and see how these modes change over time. When applied to the time series of streamflow attributes such as discharge or water temperature, WA is useful for detecting the scale-specific (e.g., annual, seasonal, or daily scale) variability and allows for the conclusions to be drawn about the causes of the flow or thermal regime alterations such as climate change, river regulation, and hydropower generation.

Despite the strength of WA in depicting flow variability at various scales, to date there are still very limited wavelet-based tools available for assessment of flow regime alterations over a spectrum of temporal scales. Three wavelet-based approaches can be found in the literature, which have been used to evaluate the deviation of the altered flow regime from the natural one. The first is the t statistics [*White et al*., 2005], which is based on a t test of the altered versus natural wavelet power spectra (here the wavelet power refers to the amplitude of flow oscillations, see section 3 for details). The t statistics has a positive value when the altered wavelet power is statistically higher than its natural counterpart, a negative value when the altered wavelet power is statistically lower, and a null value when the wavelet power remains statistically unaltered. The second is the ratio of altered GWPS (global, or time-averaged, wavelet power spectrum) to natural GWPS [*Zolezzi et al*., 2009]. A GWPS ratio greater than unity indicates an intensification of the global wavelet power, a GWPS ratio smaller than unity indicates an attenuation of the global wavelet power, and a unity ratio indicates an absence of alteration in the global wavelet power. The third is the mean absolute spectral difference [*Shiau and Huang*, 2014], defined as the time-averaged absolute differences between the altered and natural wavelet power spectra. A null value indicates that the altered and natural wavelet power spectra are fully identical, while a larger value indicates that greater deviations exist between the altered and natural wavelet power spectra.

Albeit straightforward, the above approaches were not specifically designed for use to quantify the degree of flow regime alteration. For example, the GWPS ratios = 10 (>1) and 1/10 (<1) indicate that the flow oscillations are, respectively, intensified and attenuated but do not inform us which one has a larger degree of alteration (or which one is more severely impacted), although we are informed of the fact that both are altered by an order of magnitude. Moreover, the GWPS ratio reveals only the relative change between the long-term averaged wavelet power spectra. As a result, the extremely high wavelet powers associated with rare floods could override the low wavelet powers associated with regular flows such that changes of these regular flows may be overlooked [*Shiau and Huang*, 2014]. On the other hand, the absolute nature of the t statistics and mean spectral difference prevents them from being useful for a meaningful comparison among scales since the absolute and relative deviations of wavelet power at various scales can be rather different.

To tackle the above problems, we devise a new wavelet-based approach, termed the DWPS (deviation between wavelet power spectra) approach, which is (1) able to quantify the degrees of flow regime alterations over a spectrum of temporal scales, (2) based on hour-to-hour comparisons between two wavelet power spectrum series rather than direct comparisons of two time-averaged GWPS, and (3) relative in nature rendering the output results comparable among various scales. We apply the DWPS approach to the Feitsui Reservoir system (Taiwan) for assessment of flow regime alterations. This case study offers a unique opportunity to evaluate the hydrologic impacts at three connected reaches that are subjected to different classes of anthropogenic interventions. We show that the DWPS approach reveals features that are undetectable with the GWPS ratios. We also segregate the effects of individual subflow components on the overall flow regime alterations. Note that, like any other method, our approach has its own merits and limitations (to be discussed later), thus would be most beneficial when used in combination with other wavelet-based approaches.

The remainder of this paper is structured as follows. In section 2, we provide an overview of the Feitsui Reservoir system and its operation rules. In section 3, we introduce the theoretical background of WA and two wavelet-based approaches used in this paper to assess flow regime alterations. The results are presented and discussed in section 4, which are followed by the conclusions summarized in section 5.

2. Feitsui Reservoir System

2.1. Overview

The Feitsui Reservoir system, located in northern Taiwan (Figure 1a), has been in full operation since 1987 for three main purposes: (1) domestic water supply, (2) hydropower generation, and (3) flood control [*Taipei Feitsui Reservoir Administration* (*TFRA*), 2004]. The reservoir impounds the Peishih Creek with a capacity of 460 million m^3, below the reservoir joins the Nanshih Creek, and downstream of the confluence is the Hsintien Creek. The hydropeaking power plant facilitates an annual production of 220 GWh.

Shown in Figure 1b is the flow diagram of the Feitsui Reservoir system. The inflows of the reservoir (Q_I) were recorded by the TFRA at the dam site, while the flows of the Nanshih Creek near the confluence (Q_N) were recorded by the Taiwan Power Company (TPC) at a nearby gauging station (Figure 1a). During the regular nonflood periods, three measurements (of river stage) were obtained each day at 0 A.M., 8 A.M., and 4 P.M.; only during the flood periods were the hourly records available. The flow series Q_I and Q_N, both 11 years in length (1998−2008) with a mixed 8 and 1 h resolution, were used in this study as the inputs of the flow routing. The monthly and semiannual mean runoff patterns of the Peishih and Nanshih Creeks are shown in Figure 2, where the mean runoffs of the wet semester (June–November) are, respectively, 1.9 and 2.4 times the mean runoffs of the dry semester (December–May). The annual inflow of the reservoir is ~1.1 billion m^3, while the annual runoff of the Nanshih Creek is ~1.3 billion m^3. The projected monthly domestic demands are also shown in Figure 2. The annual total demand amounts to ~1.1 billion m^3, which is jointly supplied by the unregulated flows from the Nanshih Creek (Q_N) and the flow releases from the reservoir (Q_A) (Figure 1b). The merged flows (Q_B) are diverted at the Chingtan Weir (Q_{DV}) and distributed to 4.5 million domestic users in the Taipei metropolitan area, leaving behind the postdiversion flows (Q_C).

The three connected reaches of the Feitsui Reservoir system (Figure 1b) are subjected to different classes of anthropogenic influences. Reach A, located immediately below the reservoir, is directly affected by reservoir operations/releases. Reach B, located below the confluence, receives reservoir releases and the unregulated flows from the Nanshih Creek. Reach C, located below the diversion weir, is subjected to the cumulative effect of reservoir operations, flow merging, and flow diversions. The drainage area at the Feitsui Reservoir dam site is 303 km^2 (Figure 1a), which covers ~98% of the Peishih Creek watershed at the confluence (=310 km^2), thus the inflow series Q_I recorded at the dam site was used as a proxy of the natural flow series at Reach A, $Q_{A,\mathrm{nat}}$ (Figure 1b). The drainage area at the TPC gauging station is 313 km^2, which covers 94% of the Nanshih Creek watershed at the confluence (=332 km^2); thus, the flow series Q_N recorded at the TPC gauging station was used as a proxy of the natural flow series at the confluence and the flow series Q_I+Q_N was used as a proxy of the natural flow series at Reach B, $Q_{B,\mathrm{nat}}$ (Figure 1b). The drainage area at the Chingtan Weir is 680 km^2 and the contributing area of Q_I+Q_N to this drainage area exceeds 90%; thus, the flow series Q_I+Q_N was also used as a proxy of the natural flow series at Reach C, $Q_{C,\mathrm{nat}}$ (Figure 1b). The flow series Q_A, Q_B, and Q_C were obtained using a routing model [see *Shiau and Wu*, 2013], which built upon water balance following closely the operation rules of the Feitsui Reservoir system, as described below.

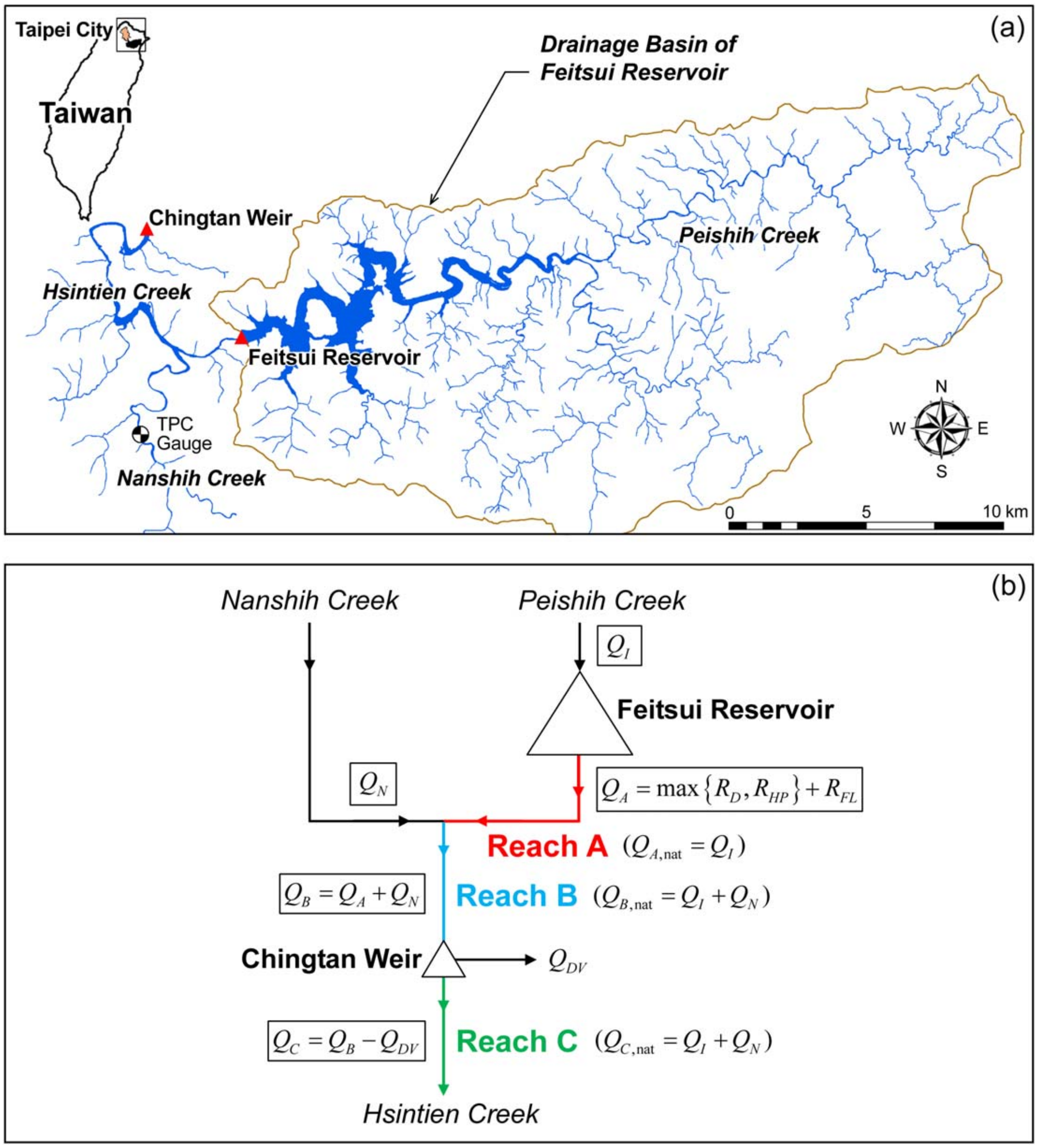

Figure 1. (a) Location map and (b) flow diagram of the Feitsui Reservoir system in northern Taiwan (dam site: 24.9°N, 121.6°E).

2.2. Operation Rules

The operation rules of the Feitsui Reservoir system are briefly summarized here. The readers are referred to *Shiau and Wu* [2013] for full details. The Feitsui Reservoir system is operated on a daily basis. The daily domestic water demand is supplied primarily by the Nanshih Creek, with the deficit supplemented by the reservoir. Figure 2 shows that during July–November the mean flows of the Nanshih Creek are sufficient to fulfill the projected water demand, while in the remaining 7 months the mean flows of the Nanshih Creek are insufficient to fulfill the projected demand. The deficits supplemented by the reservoir amount to 16% of the total demand. Each day at 0 A.M., the amount of water to be released by the reservoir for domestic water supply is determined based on the reservoir water level and concurrent flow from the Nanshih Creek. If the water level is below the lower rule curve, a hedging policy is enforced to restrict the reservoir releases by 10–30%. The amount of water so determined is evenly released in 8 h (from 8 A.M. to 4 P.M.) with a constant release rate R_D (Figure 1b).

The flow release rate R_{HP} for hydropower generation and its duration are also determined daily at 0 A.M. based on the reservoir water level. If the water level is between the upper and middle rule curves, water is

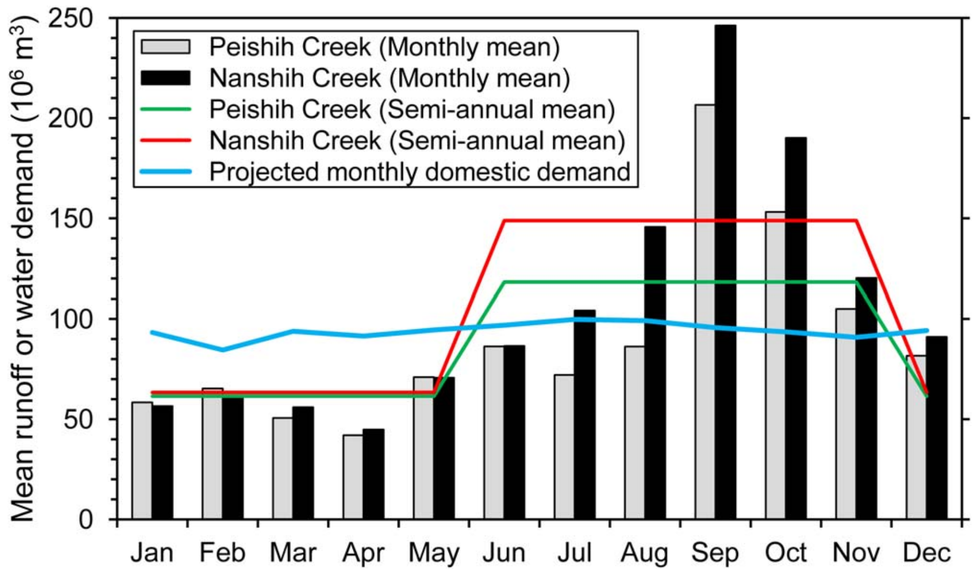

Figure 2. Monthly and semiannual mean runoff patterns of the Peishih and Nanshih Creeks along with the projected monthly domestic water demands.

released in the designated 8 h for hydropeaking power generation. If the water level exceeds the upper rule curve, a continuous release is implemented for 24 h. No flow is specifically released for hydropower generation if the water level is below the middle rule curve. An example hourly flow hydrograph (5−18 July 2000) at Reach A is given in Figure 3a, where the periodic flow pulses (daily hydropeaking) associated with the daily 8 h peaking releases during the nonflood periods and a postflood continuous release of R_{HP} during 10−13 July are demonstrated.

A three-stage compelling release of R_{FL} is implemented during the flood periods based on the reservoir inflow and water level. The first is the *antecedent flood stage*, where the compelling release is aimed to reserve a spare capacity for flood detention. The second is the *prepeak stage*, where the compelling release is aimed to attenuate flood peaks, prevent overtopping, and secure dam safety. The third is the *postpeak stage*, where the compelling release is to resume normal water levels and secure water storage available for postflood domestic water supply. The example hourly flow hydrograph given in Figure 3a shows a double-peak flood that occurred on 9 July 2000. The first peak was fully detained by the reservoir, while the second peak triggered a second-stage compelling release aiming for dam safety.

Because the flows released for domestic water supply would pass through the power plant, only the greater one between R_D and R_{HP} is released. The compelling release R_{FL}, however, is emergency dewatering through separate spillways, which occurred with a mean frequency of 5 d/yr during 1998−2008. Thus, the total release from the reservoir, Q_A, is the sum of the flows passing through the power plant and spillways, as expressed by

$$Q_A = \max\{R_D,\ R_{HP}\} + R_{FL} \tag{1}$$

At Reach B, the postconfluence flow Q_B merges the flows from Reach A and the Nanshih Creek (see the example hourly flow hydrograph given in Figure 3b), i.e.,

$$Q_B = Q_A + Q_N \tag{2}$$

The postconfluence flow Q_B is diverted at the Chingtan Weir, with the diversion rates Q_{DV} determined based on the flow Q_N from the Nanshih Creek. If Q_N is sufficient for the whole daily domestic demand, Q_{DV} is simply the diversion rate with which the daily domestic demand is evenly supplied in 24 h. If, however, Q_N alone is not sufficient for the whole daily domestic demand, Q_{DV} has a peak value in the 8 h overlapping with the release period of Q_A and a lower value in the remaining 16 h. The example hourly flow hydrograph given in Figure 3c shows that Q_{DV} remained constant during 7−15 July when Q_N were

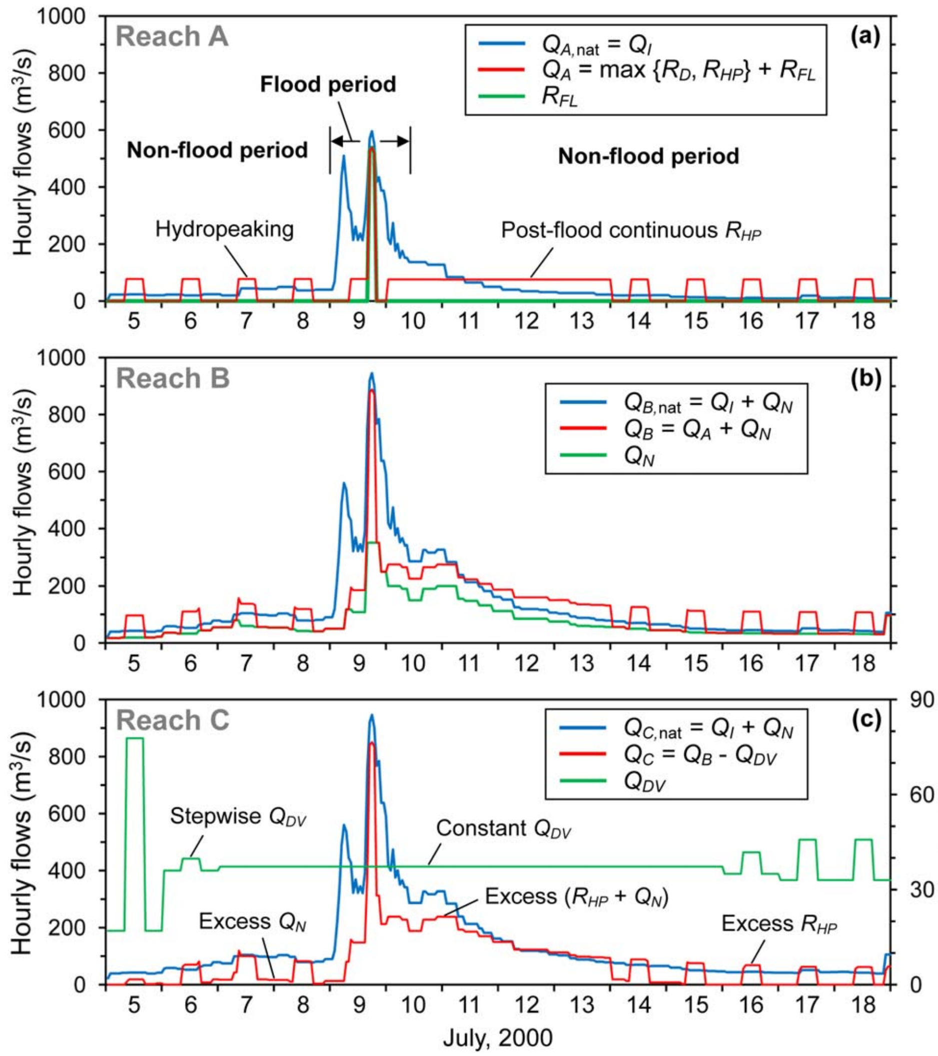

Figure 3. An example hourly hydrograph illustrating the natural and altered flow series and the subflow components at Reaches A–C (during 5−18 July 2000).

sufficient to fulfill the whole daily domestic demands, while Q_{DV} had stepwise variations in the remaining 5 days when Q_N alone were not sufficient for the whole daily domestic demands. The postdiversion flow at Reach C is given by

$$Q_C = Q_B - Q_{DV} \tag{3}$$

Here the relatively limited capacity of the weir (=3.9 million m^3), compared to that of the Feitsui Reservoir, is omitted for simplicity (see *Shiau and Wu* [2013] for details). Note also that no minimum flows are prescribed in the operation rules of the Feitsui Reservoir system [*TFRA*, 2004], resulting in a null Q_C for 56% of the time (during 1998−2008).

In this study, the altered flow series Q_A, Q_B, and Q_C were simulated using a flow routing model with the natural flow series as the inputs. To perform the flow routing on an hourly basis, the available flow series Q_I and Q_N with a mixed 8 and 1 h resolution were converted to the hourly flow series by supplementing the missing data with constant values [*Deodhar*, 2008], assuming that the regular flows during nonflood periods would not vary substantially within the 8 h intervals, while the flow data during flood periods still retained the original 1 h resolution. To verify the simulation results, the observed reservoir releases were compared with the simulated Q_A (see Appendix A for details), which shows that the simulated results coincide reasonably well with the observed results. An alternative linear interpolation for data supplement was also tested, leading to similar outcome without better justifications. The altered versus natural flow series

(Q_A, Q_B, Q_C versus $Q_{A,\mathrm{nat}}$, $Q_{B,\mathrm{nat}}$, $Q_{C,\mathrm{nat}}$) were then used to assess flow regime alterations employing two wavelet-based approaches, which are described in the following section.

3. Wavelet-Based Approaches for Assessment of Flow Regime Alterations

Two wavelet-based approaches are presented here; each approach is comprised of two stages (see Figure 4). At stage 1, the continuous wavelet transforms (CWT) of the time series are obtained at a spectrum of temporal scales. The corresponding wavelet power spectrum (WPS) series is then constructed by translating along the time axis. At stage 2, two WPS-based approaches are used to evaluate the spectral differences between two time series $Q1_n$ and $Q2_n$. The procedure of each stage is described as follows.

3.1. Stage 1: Wavelet Analysis of Time Series

The first step of stage 1 is to transform the given time series into a set of wavelet series at a spectrum of temporal scales (Figures 5a–5c). To this aim, the CWT (continuous wavelet transform) is used because it is well suited to the analysis of streamflow time series [*White et al.*, 2005; *Zolezzi et al.*, 2009; *Shiau and Huang*, 2014]. The procedure of the CWT is briefly outlined here, while further details can be found in *Torrence and Compo* [1998]. The CWT of a discrete time series x_n (for $n=0, 1, \ldots, N-1$, here $N=$ length of time series) at a given temporal scale s, denoted as $W_n(s)$, is the convolution of x_n with a wavelet function Ψ:

$$W_n(s)=\sum_{n'=0}^{N-1} x_{n'}\Psi^*\left[\frac{(n'-n)\delta t}{s}\right] \tag{4}$$

where $\Psi^*=$ complex conjugate of Ψ; $\delta t=$ data sampling interval. The convolutions are performed more efficiently in the Fourier space using a discrete Fourier transform (DFT). The readers are referred to *Torrence and Compo* [1998] for more details on the DFT. The wavelet function Ψ is obtained by normalizing a mother wavelet function Ψ_0 through $\Psi(\eta)=(\delta t/s)^{1/2}\Psi_0(\eta)$, where $\eta=(n'-n)\delta t/s=$ nondimensional time parameter. The mother wavelet function Ψ_0 adopted in this study is the Morlet function, which has been a common choice for the streamflow data [e.g., *Nakken*, 1999; *White et al.*, 2005; *Zolezzi et al.*, 2009; *Adamowski et al.*, 2009; *Shiau and Huang*, 2014], and is expressed as

$$\Psi_0(\eta)=\pi^{-1/4}e^{i\omega_0\eta}e^{-\eta^2/2} \tag{5}$$

where $\omega_0=6$ is a dimensionless wave number [*Farge*, 1992]. The schematic graphs shown in Figures 5a–5c illustrate the CWT, $W_n(s)$, at three temporal scales $s=s_1$, s_2, and s_3. These graphs show that the temporal scale s is essentially the oscillation period of $W_n(s)$.

The amplitude of $W_n(s)$, denoted as $|W_n(s)|$, may remain constant or vary with time. For example, Figures 5a and 5c show two CWT with constant amplitudes $|W_{s1}|$ and $|W_{s3}|$, while Figure 5b illustrates a CWT whose original amplitude $|W_{s2}|$ was intensified as $|W_{s3}|$ during event 1 but attenuated as $|W_{s1}|$ during event 2. The amplitude of the CWT can be used to quantify the wavelet power. The wavelet powers at a spectrum of temporal scales, termed the wavelet power spectrum (WPS), are expressed as

$$WPS_n(s)=|W_n(s)|^2 \quad \text{for } s=s_0, s_1, \ldots, s_J \tag{6}$$

By translating the WPS along the time index n, the second step of stage 1 is to construct the time series of WPS (or WPS diagram) to show the distribution of wavelet power over a spectrum of scales and how this spectral distribution varies with time. The schematic graph in Figure 5d illustrates the WPS diagram corresponding to the CWT in Figures 5a–5c. It is shown in Figure 5d that the wavelet power series at scales s_1 and s_3 remained as blue and red colored over time, while the green-colored wavelet power series at scale s_2 was changed to red and blue colored during events 1 and 2, respectively.

A set of temporal scales were used here, typically given by incremental powers of 2:

$$s_j=s_0\cdot 2^{j\cdot\delta s} \quad \text{for } j=0, 1, \ldots, J \tag{7}$$

where $s_0=$ shortest scale, constrained by data resolution (=sampling interval δt), a value of $2\delta t$ has been suggested [*Zolezzi et al.*, 2009]. The input hourly flow series used in this study were converted from the time series with a mixed 8 and 1 h resolution, thus the shortest resolvable scale s_0 would be 16 h rather than 2 h.

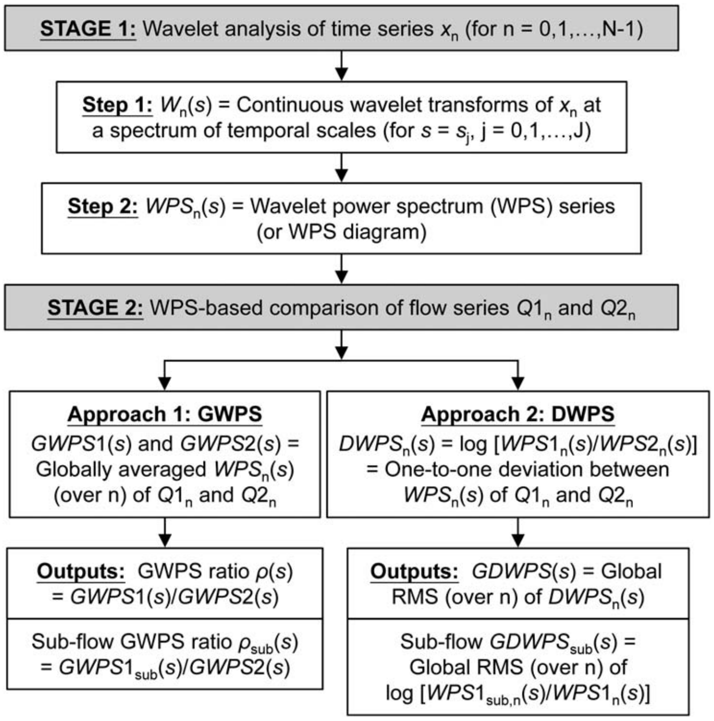

Figure 4. Flowchart of wavelet analysis and two WPS-based approaches for comparison of flow series $Q1_n$ and $Q2_n$. The first approach is based on the global wavelet power spectrum (GWPS), with the outputs being the GWPS ratios and subflow GWPS ratios. The second approach is based on the one-to-one deviation between wavelet power spectra (DWPS) series, with the outputs being the global deviation between wavelet power spectra (GDWPS) and subflow GDWPS.

A scale-sampling interval $\delta s=0.05$ was used to produce a smooth WPS; J determines the longest scale s_J, a value of s_J shorter than 10% of the data length has been recommended [*Percival and Walden*, 2000; *Steel and Lange*, 2007]. In this study, the length of the available data is 11 years, giving the longest reliable scale of 1 year.

3.2. Stage 2: WPS-Based Comparison of Time Series

Two WPS-based approaches were used to compare any two flow series $Q1_n$ and $Q2_n$ and evaluate the spectral differences between these flow series. The first approach is based on the global wavelet power spectrum (GWPS), presented earlier by *Zolezzi et al*. [2009]; the second approach is a new one devised in this work based on the deviation between wavelet power spectra (DWPS). These approaches are described as follows.

3.2.1. GWPS Approach

The time average of WPS over the entire data length, termed the global (or globally averaged) wavelet power spectrum (GWPS), denoted as $GWPS(s)$, is expressed as

$$GWPS(s)=\frac{1}{N}\sum_{n=0}^{N-1}WPS_n(s)=\frac{1}{N}\sum_{n=0}^{N-1}|W_n(s)|^2 \quad \text{for } s=s_0, s_1, \ldots, s_J \tag{8}$$

This time averaging may be also performed over each year or season to generate an annually averaged WPS (AWPS) series or seasonally averaged WPS (SWPS) series that reveals the annual or seasonal alteration trend. In this study, we focused on the global spectral differences between $Q1_n$ and $Q2_n$. To compare the GWPS of $Q1_n$ and $Q2_n$, a GWPS ratio $\rho(s)$ may be used [*Zolezzi et al*., 2009], which is given by

$$\rho(s)=\frac{GWPS1(s)}{GWPS2(s)} \quad \text{for } s=s_0, s_1, \ldots, s_J \tag{9}$$

where $GWPS1(s)$ and $GWPS2(s)=$ GWPS of $Q1_n$ and $Q2_n$, respectively. The GWPS ratios so calculated range between [0, ∞]. A value of $\rho(s)>1$ indicates that at scale s the global wavelet power of $Q1_n$ is greater than that of $Q2_n$, more specifically, the global amplitude of CWT at scale s is greater for $Q1_n$ than for $Q2_n$. In case where $Q1_n$ and $Q2_n$ represent the altered and natural flow series, respectively, $\rho(s)>1$ means that at scale s the altered flow regime has intensified flow oscillations (or higher powers), while $\rho(s)<1$ means that the altered flow regime has attenuated oscillations (or lower powers). By plotting the profile of $\rho(s)$, it is easy to distinguish intensified flow oscillations from attenuated ones and identify the temporal scales at which the relative change in global wavelet power (or amplitude of flow oscillations) is most notable.

The altered flow series $Q1_n$ may comprise a number of subflow components. For example, Figure 1b shows that the postconfluence flow Q_B is comprised of Q_A and Q_N. To segregate the effect of each subflow component $Q1_{\mathrm{sub},n}$, we define a subflow GWPS ratio $\rho_{\mathrm{sub}}(s)$ as follows:

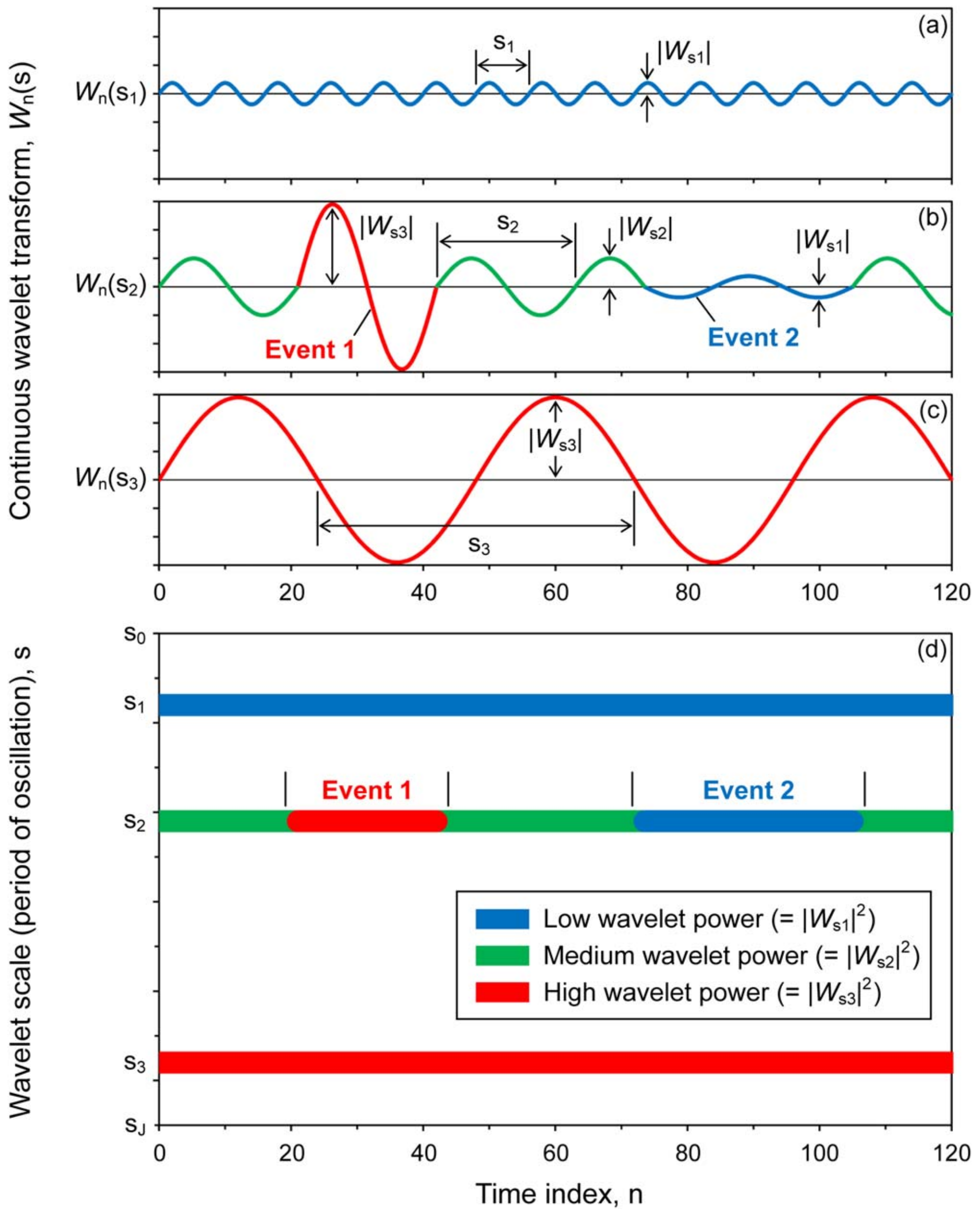

Figure 5. Schematic graphs showing the procedure of wavelet analysis: (a–c) continuous wavelet transforms (CWT) at three temporal scales s_1, s_2, and s_3, and (d) the corresponding WPS diagram.

$$\rho_{sub}(s)=\frac{GWPS1_{sub}(s)}{GWPS2(s)} \quad \text{for } s=s_0, s_1, \ldots, s_J \tag{10}$$

where $GWPS1_{sub}(s)=$ GWPS derived from subflow series $Q1_{sub,n}$. Similarly, by plotting the profile of $\rho_{sub}(s)$, the contributions of each subflow component to the alterations of time-averaged flow regime at various scales, i.e., $\rho(s)$, may be unraveled.

The GWPS ratios provide a quick indication of intensified/attenuated flow oscillations at a spectrum of temporal scales. They were, however, not designed for use to quantify the degrees of flow regime alteration at these scales (as noted in section 1). In addition, the GWPS ratios reveal only the relative changes of the long-term averaged WPS. They lack the information regarding individual WPS deviations derived from one-to-one (i.e., *n*-to-*n*) comparisons of two WPS series. As such, some extremely high wavelet powers could override the low wavelet powers in the process of time averaging, so that changes of the latter are often overlooked. This motivates us to devise a new tool for quantifying the degree of flow regime alteration based on individual WPS deviations.

3.2.2. DWPS Approach

To evaluate the spectral differences between flow series $Q1_n$ and $Q2_n$, the one-to-one (i.e., hour-to-hour in this study) deviation between wavelet power spectra (DWPS) series, denoted as $DWPS_n(s)$, is calculated first:

$$DWPS_n(s) = \log \frac{WPS1_n(s)}{WPS2_n(s)} \quad \text{for } s = s_0, s_1, \ldots, s_J \tag{11}$$

where $WPS1_n(s)$ and $WPS2_n(s) =$ WPS series of $Q1_n$ and $Q2_n$. The log operation is to ensure that DWPS = 0 when the WPS ratio is equal to 1, and the DWPS has a large positive or negative value when the WPS ratio deviates much from 1. The root-mean-square (RMS) of $DWPS_n(s)$ is then performed over time to yield the global DWPS (GDWPS):

$$GDWPS(s) = \underset{n=0}{\overset{N-1}{\mathrm{RMS}}} \left(DWPS_n(s) \right) = \left[\frac{1}{N} \sum_{n=0}^{N-1} \left(\log \frac{WPS1_n(s)}{WPS2_n(s)} \right)^2 \right]^{1/2} \quad \text{for } s = s_0, s_1, \ldots, s_J \tag{12}$$

The RMS operation is to ensure that positive and negative DWPS would not cancel each other out. The GDWPS so calculated ranges between [0, ∞]. The GDWPS has a large positive value when the one-to-one WPS ratios deviate much from 1 whereas the GDWPS has a minimum value of 0 if the one-to-one WPS ratios are all equal to 1, rendering the GDWPS useable as a metric to indicate explicitly the degree of spectral deviation between $Q1_n$ and $Q2_n$ without distinguishing between intensified and attenuated flow oscillations (i.e., positive and negative DWPS). In addition, the relative nature of the GDWPS (via the WPS ratios) allows for a comparison among different scales. By plotting the profile of $GDWPS(s)$, it is easy to identify the temporal scales at which the relative deviations between individual WPS are most notable.

Given that $Q1_{sub,n}$ is a subflow component of the altered flow series $Q1_n$, we define a subflow GDWPS, $GDWPS_{sub}(s)$, to segregate the effect of the subflow component:

$$GDWPS_{sub}(s) = \left[\frac{1}{N} \sum_{n=0}^{N-1} \left(\log \frac{WPS1_{sub,n}(s)}{WPS1_n(s)} \right)^2 \right]^{1/2} \quad \text{for } s = s_0, s_1, \ldots, s_J \tag{13}$$

where $WPS1_{sub,n}(s) =$ WPS series derived from $Q1_{sub,n}$. The subflow GDWPS also ranges between [0, ∞] and may well be interpreted as the spectral deviations of $Q1_{sub,n}$ from $Q1_n$. A value of $GDWPS_{sub}(s)$ close to zero indicates that $Q1_{sub,n}$ resembles closely $Q1_n$ (or $Q1_{sub,n}$ is well representative of $Q1_n$) at scale s, whereas a large positive value of $GDWPS_{sub}(s)$ indicates that $Q1_{sub,n}$ and $Q1_n$ have poor resemblances at scale s. By plotting the profile of $GDWPS_{sub}(s)$, the relative dominances of each subflow component on the GDWPS of $Q1_n$ and $Q2_n$ at various scales may be unraveled.

It should be noted that different terms are used here to normalize the subflow effects in the definitions of $\rho_{sub}(s)$ and $GDWPS_{sub}(s)$, which are the natural consequences of the differences behind the origins of the GWPS and DWPS approaches. As such, comparison of $\rho_{sub}(s)$ and $GDWPS_{sub}(s)$ should proceed with care where similar messages may be delivered by these metrics confirming each other or otherwise unique information may be revealed by each metric demanding a synthesis of interpretations.

4. Results and Discussion

4.1. Natural and Altered WPS

The WPS-related results associated with the natural and human-impacted flow series of Reaches A−C are given in Figures 6 and 7. For Reach A, the hourly inflows and outflows of the reservoir (Q_I and Q_A series) are shown in Figures 6a and 6d, respectively, where the more variable pattern of reservoir inflows is replaced by a much less variable pattern of regular, daily hydropeaking waves, except those compelling releases during the flood periods. The WPS diagrams of Q_I and Q_A series are shown in Figures 6b and 6e, respectively. The former demonstrates a smooth transition from high-frequency low-power oscillations (in the upper part) to low-frequency high-power oscillations (in the lower part), with a number of exceptions where the high-power events (red spikes that reach to the top of the graph) associated with large floods affected the wavelet powers over all scales. This variation trend is revealed also by the GWPS in Figure 6c,

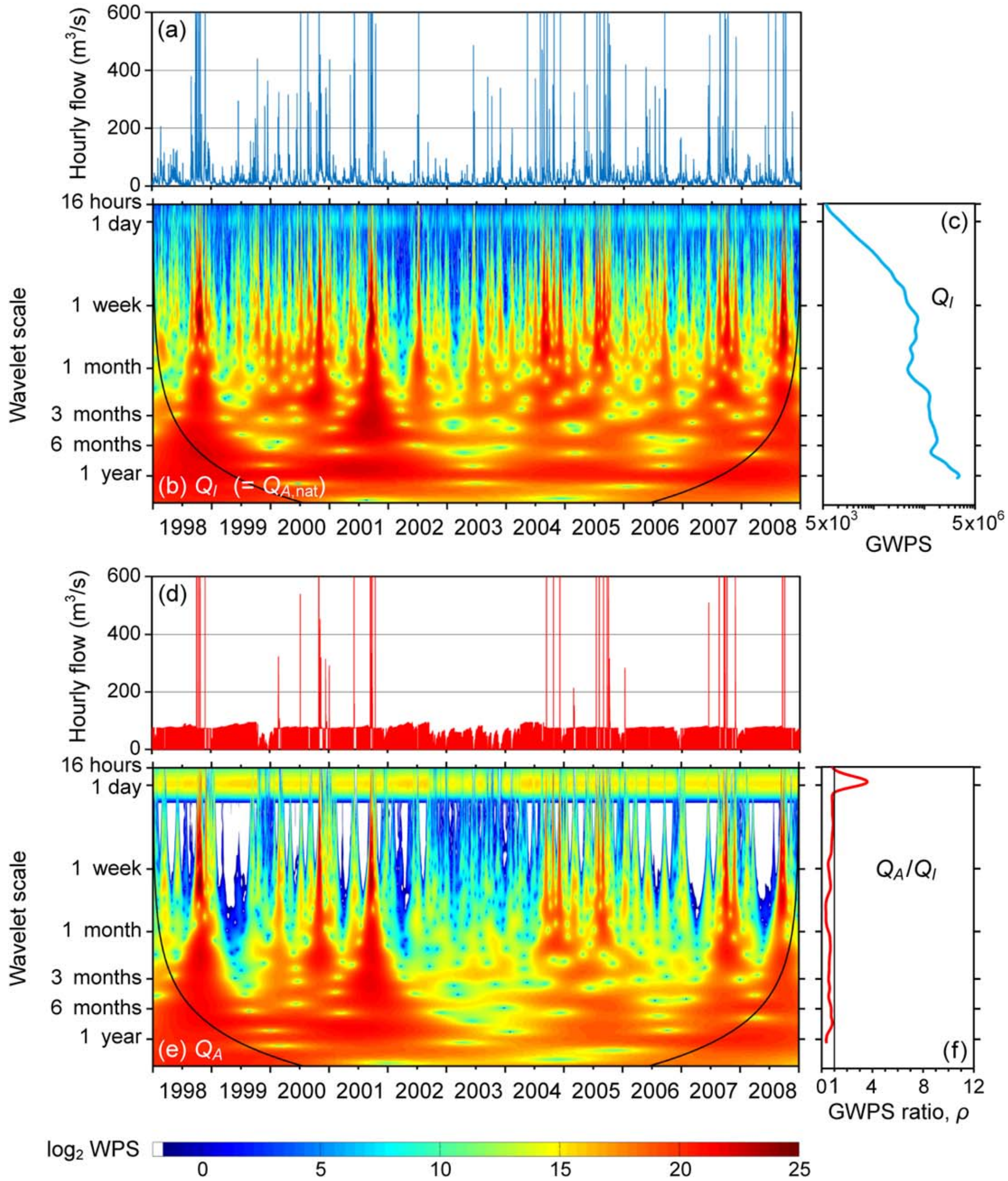

Figure 6. (a and d) Hourly inflow Q_I and outflow Q_A series of the Feitsui Reservoir (truncated at 600 m^3/s); (b and e) WPS diagrams of Q_I and Q_A; (c) GWPS of Q_I; (f) GWPS ratio of Q_A to Q_I. Base-2 logarithms of WPS are shown in Figures 6b and 6e in terms of color scale, where the white swaths indicate that the logarithmic WPS are smaller than -2.

where the global wavelet power increased by nearly 3 orders of magnitude when varying from subdaily to annual scale.

The altered WPS diagram of Reach A (Figure 6e) exhibits two qualitative features that are not observed in the natural one (Figure 6b), which include (1) a persistent yellow band present at daily scale, which is occasionally interrupted by very high or low powers associated with the large compelling releases or enforced restricted water releases; (2) quite a few white swaths present between 2 days and monthly scales (in particular at subweekly scales), which represent very low powers with their logarithmic WPS being smaller than -2. The GWPS ratio of Q_A to Q_I is given in Figure 6f, which shows that the daily-scale yellow band is the only one with $\rho > 1$, indicating that the flow oscillations associated with the daily hydropeaking waves are the only

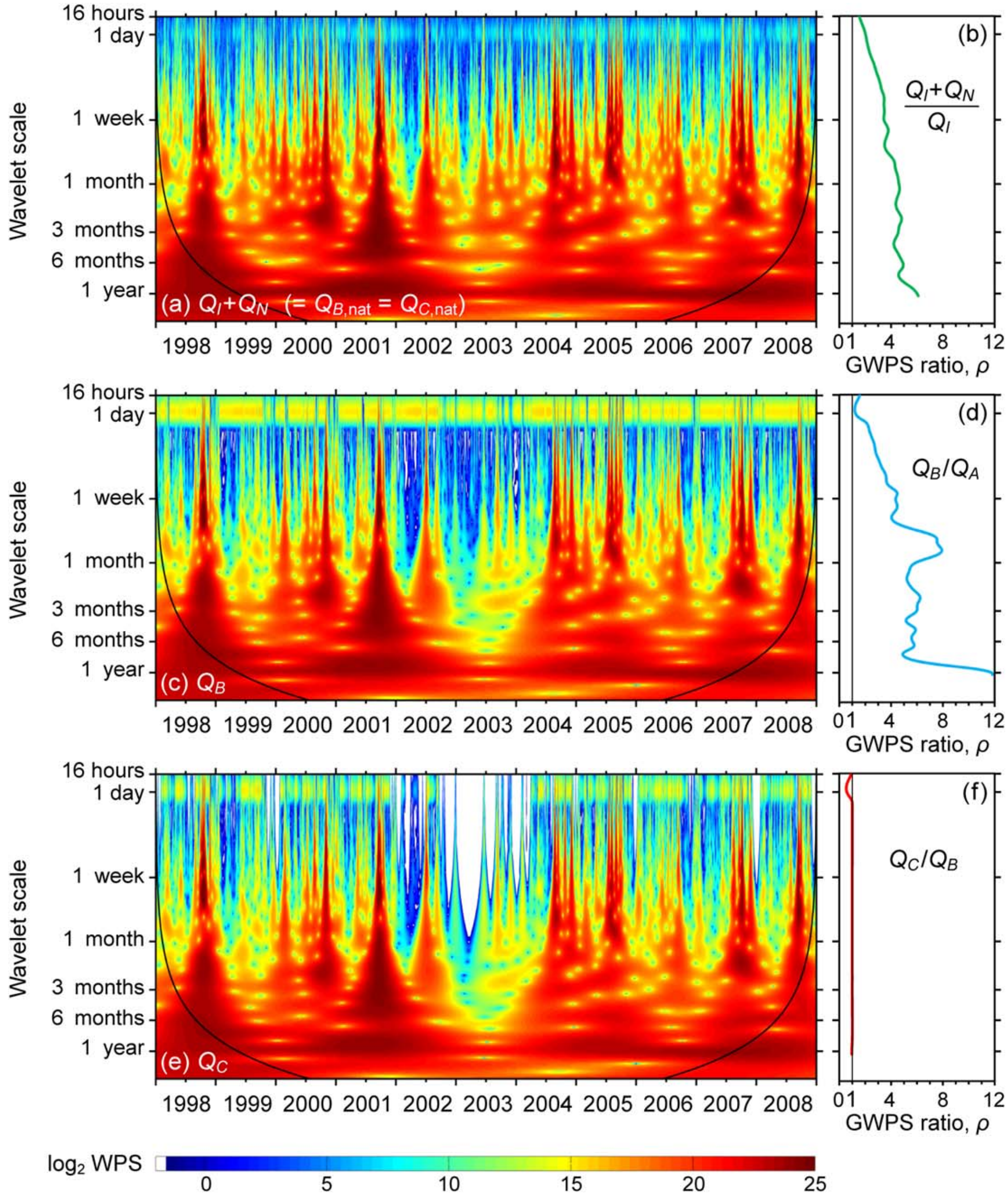

Figure 7. (a, c, and e) WPS diagrams of Q_I+Q_N, Q_B, and Q_C; (b, d, and f) GWPS ratios of Q_I+Q_N to Q_I, Q_B to Q_A, and Q_C to Q_B. Base-2 logarithms of WPS are shown in Figures 7a, 7c, and 7e in terms of color scale, where the white swaths indicate that the logarithmic WPS are smaller than -2.

one intensified with reservoir operations. The values of ρ at the remaining scales are consistently smaller than unity. The white swaths at subweekly scales, however, did not lead to particularly low values of ρ.

For Reaches B−C, the WPS diagram of the natural flows (Q_I+Q_N series) is shown in Figure 7a, which largely resembles the WPS diagram of Q_I series (Figure 6b) but in general has higher powers than Q_I due to the joining of Q_N. This is evidenced by the GWPS ratio of Q_I+Q_N to Q_I (Figure 7b), where the GWPS ratio is consistently greater than unity, and exhibits an increasing trend with the scale. The altered WPS diagram of Reach B is shown in Figure 7c, which resembles Figure 6e, exhibiting also a yellow band at daily scale. However, due to the joining of Q_N, the subweekly scale white swaths are significantly reduced. Moreover, the altered WPS diagram of Reach B exhibits consistently higher powers than its preconfluence counterpart shown in Figure 6e. This is evidenced by the GWPS ratio of Q_B to Q_A given in Figure 7d, where the GWPS ratio is consistently greater than unity. Only at daily scale is the GWPS ratio close to unity, indicating that the oscillations of Q_A associated with daily hydropeaking waves were not changed much with the joining of the unregulated flows Q_N.

The altered WPS diagram of Reach C is given in Figure 7e, which generally resembles Figure 7c but exhibits two main differences: (1) the wavelet power of the daily-scale band is reduced; (2) the white swaths are present at times different from those observed in Figures 6e and 7c, and the white swaths in Figure 7e are not truncated by the daily-scale band as seen in Figures 6e and 7c. The GWPS ratio of Q_C to Q_B is given in Figure 7f, where only at daily scale is the GWPS ratio smaller than unity, the GWPS ratios at the remaining scales are extremely close to unity. These indicate that the global wavelet power associated with daily hydropeaking waves was attenuated with the diversion of Q_{DV} but was not fully eliminated, whereas the GWPS at the remaining scales was essentially unaffected. The difference in the pattern of white swaths indicates that the cause of the white swaths in Figure 7e may differ from the cause of those in Figures 6e and 7c.

In this section, qualitative observations of the reach-wise natural and altered WPS diagrams are presented, which are supplemented by the ratios of downstream to upstream GWPS that show the spectral changes of the long-term natural and altered flow regimes along the river reaches. In the following section, the ratios of altered to natural GWPS are used to assess the alterations of time-averaged flow regimes along the river reaches, and the subflow GWPS ratios are used to unravel the contributions of each subflow component.

4.2. Assessment of Flow Regime Alterations Using GWPS Ratios

The GWPS ratios of altered to natural flows at Reaches A−C are shown in Figures 8a, 8d, and 8g, respectively. These results exhibit a common feature: the GWPS ratio is greater than unity solely at daily scale. Such result delivers a message: the intensified daily-scale oscillations of Q_A are carried over to the downstream reaches, which is consistent with the results seen in Figures 7c and 7e. The daily-scale GWPS ratio reduces from 3.6 (Reach A) to 2.2 (Reach B) to 1.2 (Reach C), indicating that joining of the unregulated tributary flows Q_N reduces the relative amplitude of daily-scale flow oscillations to the natural flows, and diversion of Q_{DV} further reduces the relative amplitude of daily-scale flow oscillations to the natural flows. These are indirectly consistent with the results shown in Figures 7b, 7d, and 7f because the GWPS ratio in Figure 8d divided by the GWPS ratio in Figure 8a is equal to the GWPS ratio in Figure 7d divided by the GWPS ratio in Figure 7b, and the GWPS ratio in Figure 8g divided by the GWPS ratio in Figure 8d is equal to the GWPS ratio in Figure 7f. In contrast to the reach-wise decreasing trend of the daily-scale flow oscillations, the GWPS ratio of altered to natural flows at the remaining scales is increased from Reaches A and B but held unchanged from Reaches B and C, which are also consistent with the results shown in Figures 7b, 7d, and 7f.

For Reach A, the subflow GWPS ratios of $\max\{R_D,\ R_{HP}\}$ and R_{FL} to $Q_{A,\,\mathrm{nat}}$ are shown in Figures 8b and 8c, respectively. The former reveals that the regular daily releases for domestic water supply and hydropower generation are the sole contributor to the intensified flow oscillations at daily scale, while the effects of these regular daily releases on the global wavelet powers at the remaining scales are minimal. In contrast, the subflow GWPS ratio of R_{FL} to $Q_{A,\,\mathrm{nat}}$ reveals that the compelling releases for flood control, compared to the natural flows, exhibit consistently attenuated flow oscillations at all scales.

For Reach B, the subflow GWPS ratios of Q_A and Q_N to $Q_{B,\,\mathrm{nat}}$ are shown in Figures 8e and 8f, respectively. Figure 8e reveals that the intensified oscillations of Q_B at daily scale were inherited from the daily-scale oscillations of Q_A, while Figure 8f exhibits a nearly constant ratio of 0.27, indicating that the oscillations of Q_N were proportionally in phase with the oscillations of the natural flows Q_I+Q_N at all scales. The attenuated oscillations of Q_B at the remaining scales were not attributed solely to Q_A or Q_N. Instead, they arose from the combined effects of Q_A and Q_N.

For Reach C, the subflow GWPS ratios of Q_B and $-Q_{DV}$ to $Q_{C,\,\mathrm{nat}}$ are shown in Figures 8h and 8i, respectively. Note that the WPS series of Q_{DV} and $-Q_{DV}$ are identical because the CWT of Q_{DV} and $-Q_{DV}$ have the same amplitudes of oscillations. The subflow GWPS ratio of Q_B to $Q_{C,\,\mathrm{nat}}$ (Figure 8h) coincides with the GWPS ratio of Q_C to $Q_{C,\,\mathrm{nat}}$ (Figure 8g) except at daily scale where the former has a greater value, with their difference being attributed to the subflow GWPS ratio of $-Q_{DV}$ to $Q_{C,\,\mathrm{nat}}$ (Figure 8i). Such results clearly indicate that the daily-scale oscillations of Q_B were attenuated with the diversion of Q_{DV}, and these flow

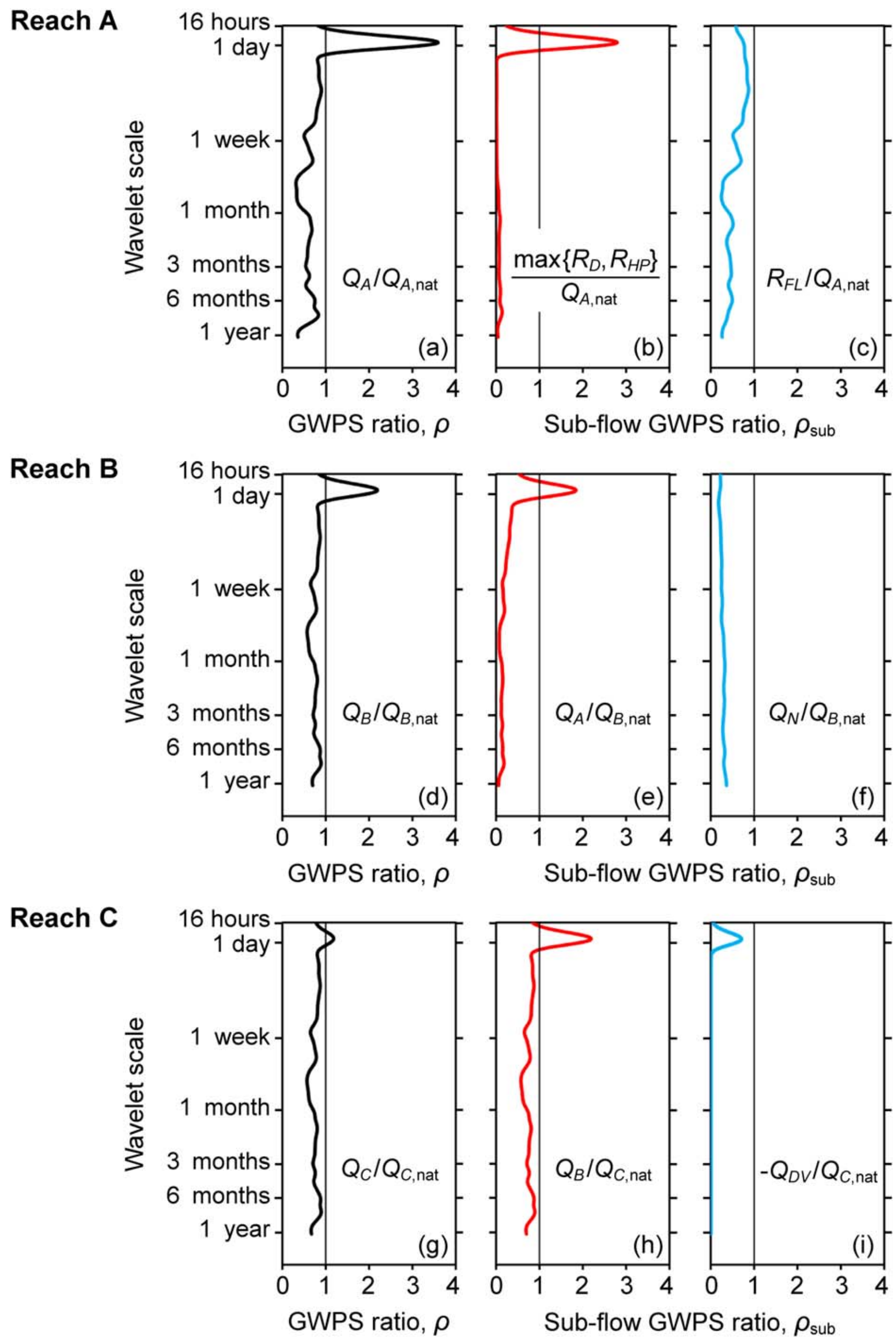

Figure 8. (a, d, and g) GWPS ratios; (b, c, e, f, h, and i) subflow GWPS ratios of Reaches A−C.

diversions hardly had any effects on the variability of Q_C at the remaining scales, where $-Q_{DV}$ exhibits null global wavelet powers.

In this section, we show that the GWPS ratio may be used as a quick indicator of flow regime alteration, in particular concerning the intensification or attenuation of global wavelet powers at various scales. However, because the time-averaged WPS is used, the GWPS ratio can only be viewed as a "ratio of two means." The natural and altered flow regimes are represented by two GWPS that may not be very representative when the standard deviations of the time series are extremely large. This is particularly true in our case, where a large number of regular flows on the order of 1−10 m^3/s are interspersed with rare floods on the order of

10^2-10^3 m^3/s. For example, the natural and altered flow series of Reach A (shown in Figures 6a and 6d) had very similar means (34.20 and 34.03 m^3/s) despite their significant differences. Likewise, the natural and altered flow series of Reach B also had similar means (74.60 and 74.43 m^3/s) that only differed by 0.2%. As a result, the extremely high powers of rare floods can override the low powers of frequent regular flows, such that alterations of regular flow regimes are often overlooked.

4.3. Assessment of Flow Regime Alterations Using GDWPS

The GDWPS of the altered versus natural flow series at Reaches A−C are, respectively, shown in Figures 9a, 9d, and 9g. At Reach A, Figure 9a exhibits a primary peak at 2 day scale along with significant GDWPS at subweekly scales and a secondary peak at daily scale, indicating that the altered flow regime had primary spectral deviations from the natural one at subweekly scales and a secondary spectral deviation at daily scale. The declining trend with the scale further suggests that those lower-frequency higher-power flow regimes are more difficult to manipulate with the reservoir operations [*Shiau and Wu*, 2010, 2013]. By comparing Figure 9a with the WPS diagrams (Figures 6b and 6e) we may come to a quick conclusion: the secondary peak of GDWPS at daily scale is due to the yellow band associated with daily hydropeaking waves, as already demonstrated in Figure 8a. As for the primary spectral deviations at subweekly scales, close inspection of Figures 6b and 6e reveals that the many white swaths at this range of scales may be responsible for such outcome. Two questions are thus raised here: (1) why are such white swaths present in particular at subweekly scales? (2) Why are these white swaths truncated consistently by the daily-scale yellow band?

To answer these questions, we conduct a numerical experiment by generating a set of flows that are released with two temporal patterns: one released regularly with a 1 day period, the other released randomly with a 1 day cycle (see Appendix B). The experiment reveals that the regular releases would result in a WPS that only exhibits high powers at daily scale, while the random releases would result in a WPS exhibiting not only the daily-scale high powers but also significant powers at subweekly scales. The spectral differences between these two time series are most notable at subweekly scales, where the extreme GWPS ratio and peak GDWPS are both present at 2 day scale. Based on this we conclude: the white swaths present at subweekly scales (Figure 6e) are attributable to the strictly periodic hydropeaking waves associated with daily releases for domestic water supply and hydropower generation. Such daily hydropeaking waves would eliminate flow oscillations at the neighboring scales, resulting in low wavelet powers and thus white swaths in particular at subweekly scales. The daily hydropeaking waves also create a clear-cut high-power band at daily scale with an abrupt drop of power present at 2 day scale, such that the low-power white swaths appear as if truncated by the daily-scale high-power band.

The primary spectral differences at subweekly scales (Figure 9a) are not revealed by the GWPS ratio (Figure 8a) because the extremely high powers associated with rare floods or compelling releases overrode the low powers associated with natural regular flows (Figure 6b) or even lower powers associated with daily hydropeaking waves (Figure 6e) in the process of time averaging, rendering the GWPS ratios (Figure 8a) at subweekly scales only slightly smaller than unity. In contrast, the one-to-one logarithmic ratios of altered to natural WPS are root-mean-squared over time to calculate the GDWPS; thus, the GDWPS may be interpreted as a "sum of relative spectral deviations" because individual spectral difference between each pair of data is actually taken into account. Elimination of subweekly flow variability due to reservoir operations has been reported recently [*Botter et al*., 2010; *Matos et al*., 2010]. Such alteration of subweekly-scale flow regimes can be detrimental because impacts on aquatic biota caused by changes in physical habitat may not be in phase with daily hydropeaking waves due to the longer time scales (subweekly to submonthly scales) required for channel and habitat adjustments [*Bunn and Arthington*, 2002; *Arthington and Sternberg*, 2012]. This combined effect of flow regime and habitat alterations at subweekly scales merits future studies.

To unravel the dominance of each subflow component on the overall GDWPS (Figure 9a), we show in Figures 9b and 9c the subflow GDWPS of max$\{R_D, R_{HP}\}$ versus Q_A and R_{FL} versus Q_A. Figure 9b reveals that the spectral deviations between max$\{R_D, R_{HP}\}$ and Q_A are consistently small at all scales, while Figure 9c reveals that the spectral deviations between R_{FL} and Q_A are generally much greater except at the longest scales. These results suggest that the flow regime alterations of Reach A were essentially dominated by the daily releases for domestic water supply and hydropower generation, whereas the compelling releases for flood control had notable hydrologic impacts only between semiannual and annual scales.

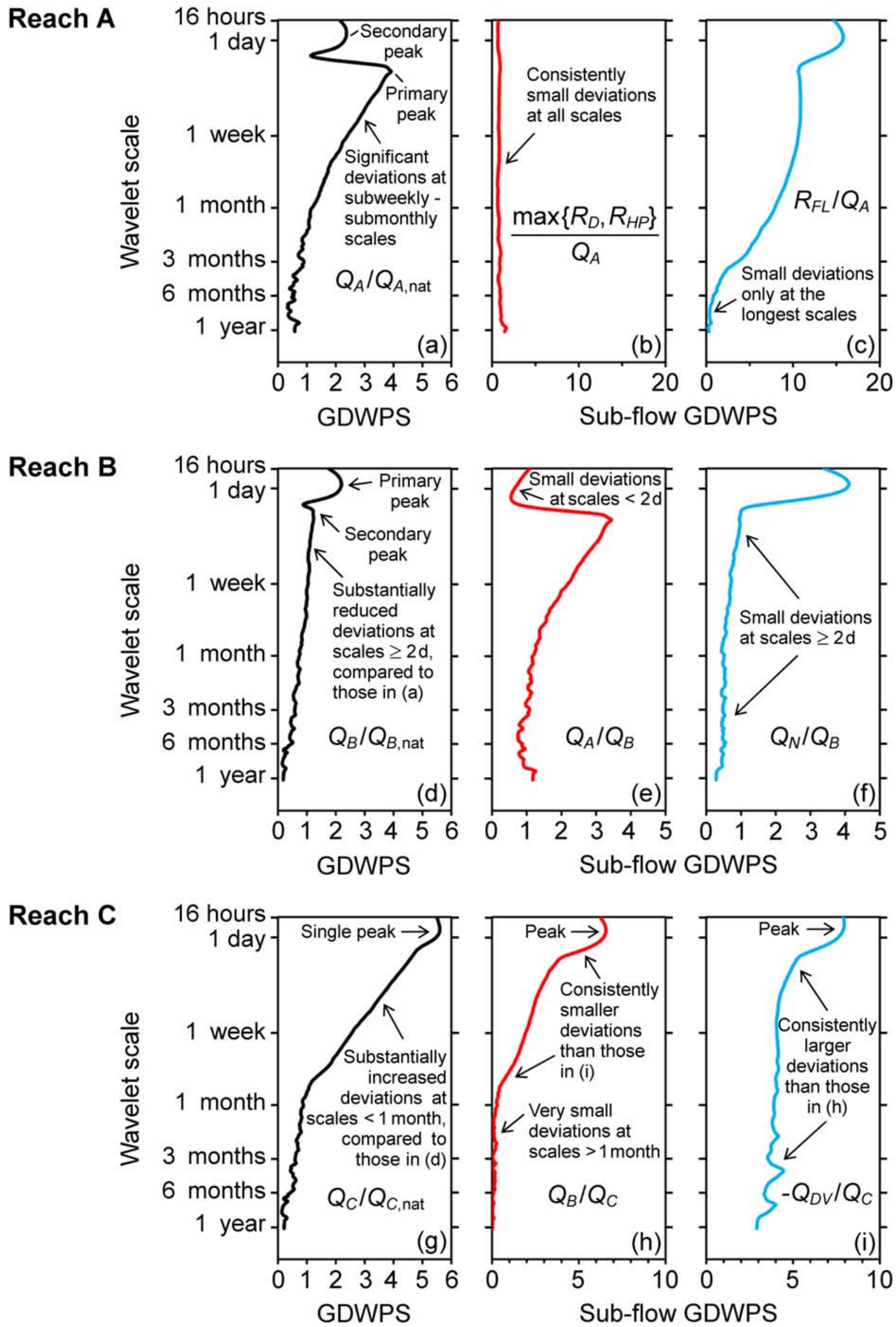

Figure 9. (a, d, and g) GDWPS; (b, c, e, f, h, and i) subflow GDWPS of Reaches A−C.

At the postconfluence Reach B, the GDWPS (Figure 9d) exhibits a primary peak at daily scale and a secondary peak at 2 day scale. Compared to Figure 9a, the GDWPS at scales $\geq$ 2 days are consistently reduced. Inspection of Figure 7c reveals a much smaller amount of white swaths in comparison to Figure 6e, which substantially reduced the GDWPS at submonthly scales (Figure 9d). To unravel the effects of each subflow component on these observed features, we show in Figures 9e and 9f the subflow GDWPS of Q_A versus Q_B and Q_N versus Q_B. A comparison of Figures 9e and 9f reveals that the spectral deviations between Q_A and Q_B are smaller at scales shorter than 2 days, whereas the spectral deviations between Q_N and Q_B are smaller at scales $\geq$ 2 days. These results indicate that the primary flow regime alteration at daily scale (Figure 9d) is attributed to the daily hydropeaking waves inherited from Q_A, which is consistent with the finding from Figure 8e, whereas the reduced flow regime alterations at scales ≥ 2 days are attributable to the joining of the unregulated tributary flows Q_N.

The GDWPS of the postdiversion Reach C (Figure 9g), compared to that of Reach B, exhibits a much greater single peak at daily scale, increased GDWPS at submonthly scales and nearly unaltered GDWPS at the longer scales. The increased GDWPS at daily scale is contrary to the reduced GWPS ratio observed between Reaches B and C (Figures 8d and 8g), the increased GDWPS at submonthly scales also differ from the corresponding GWPS ratios that remained unaltered between Reaches B and C. Inspection of Figure 7e reveals that the increased GDWPS at subdaily to monthly scales are attributed to the increased amount of white swaths compared to Figure 7c, and the pattern of these white swaths differ from those observed in Figures 6e and 7c. Two major differences are identified: (1) the white swaths are present at times when restricted water releases were enforced due to very low reservoir stages during severe droughts, and (2) the white swaths are not truncated by the daily-scale high-power band. These white swaths are observed mainly in 2003, where the restricted reservoir releases and the resulting null postdiversion flows Q_C could last for months, creating continuous, untruncated white swaths over subdaily to monthly scales.

To unravel the subflow effects on the postdiversion GDWPS, we show the subflow GDWPS of Q_B versus Q_C and $-Q_{DV}$ versus Q_C in Figures 9h and 9i. A comparison of Figures 9h and 9i reveals that the spectral deviations between $-Q_{DV}$ and Q_C are consistently larger than those between Q_B and Q_C, indicating that in general the postdiversion GDWPS is dominated by Q_B rather than $-Q_{DV}$. In particular, the spectral deviations between Q_B and Q_C are close to 0 at scales longer than 1 month, implying that $-Q_{DV}$ had no effect on the flow regimes at this range of scales. However, the subflow GDWPS of Q_B versus Q_C and $-Q_{DV}$ versus Q_C both peak at daily scale, where these two peaks have similar values ($\sim$7–8), suggesting that the postdiversion flow regime at daily scale is not attributed solely to Q_B or $-Q_{DV}$. Rather, the daily-scale flow regime was the common result of Q_B and $-Q_{DV}$, consistent with the finding from Figures 8h and 8i. In other words, the residual hydropeaking waves associated with the excess releases for hydropower generation give rise to the peak GDWPS observed at daily scale (see the example hourly flow hydrograph in Figure 3c).

5. Conclusions

We used two wavelet-based approaches to assess the flow regime alterations over a spectrum of temporal scales ranging from subdaily to annual. Our study site included three connected river reaches subjected to different classes of anthropogenic interventions, thus offered a unique opportunity to test the spatial responsiveness of these approaches. The first approach is based on the ratio of altered to natural GWPS, which delivers quick messages that are straightforward and simple. Specifically, the daily-scale flow oscillations associated with the daily hydropeaking waves was the solely intensified flow regime under the current rules of reservoir operation; this daily-scale flow variability was attenuated with the joining of the unregulated tributary flows and further attenuated by the downstream flow diversions. However, because the low powers associated with regular flows were overridden by the extremely high powers associated with rare floods or compelling releases in the process of time averaging, some important information was lost by these GWPS ratios.

The second approach, based on the GDWPS that is the root-mean-squared one-to-one logarithmic ratios of altered to natural WPS, provided new information not revealed by the GWPS ratios. The GDWPS is able to indicate the degree of flow regime alteration but does not distinguish between intensified and attenuated flow variability. In summary, the largest GDWPS observed at the postdiversion reach indicate that flow regimes were most severely altered by water abstraction, where the residual hydropeaking waves associated with the excess releases for hydropower generation were responsible for the peak GDWPS at daily scale, while the null postdiversion flows associated with the restricted releases were responsible for the large GDWPS over submonthly scales. The second largest GDWPS observed at the below-reservoir reach indicate that the strictly periodic, daily hydropeaking not only caused the daily-scale flow regime alteration but also eliminated the subweekly flow variability, leading to significant flow regime alterations over submonthly scales. The smallest GDWPS observed at the postconfluence reach indicate that flow regime alterations at scales longer than 2 days were substantially mitigated with the joining of the unregulated tributary flows while the daily-scale flow regime alteration was retained due to the daily hydropeaking inherited from the reservoir releases.

Based on these results, some practical water management strategies are recommended to sustain the natural flow variability. First, a continuous release rather than a pulse release may be implemented to eliminate the daily hydropeaking below a reservoir. Second, in case a pulse-type daily release is to be used, then a randomly arranged (or unevenly spaced) release pattern instead of a regularly arranged (or strictly periodic) release pattern is preferred to avoid full elimination of the subweekly flow variability. Third, a downstream diversion pattern that adapts to the upstream excess releases is demanded in order to mitigate the residual daily hydropeaking at the postdiversion reach. Fourth, minimum flow prescriptions should be mandated to prevent null postdiversion flows and elimination of natural flow variability over submonthly scales particularly during the drought periods.

Further studies are currently undertaken to seek the optimal scale-targeted reservoir operation scenarios based on the scale-specific GDWPS. The subflow GDWPS can be a useful tool for segregating the hydrologic impacts of individual subflow components that could help identify what and how potential modifications of operation rules can be made to mitigate the critical impacts at specific temporal scales and spatial locations. The proposed DWPS approach, when used in combination with the GWPS approach, would provide more comprehensive information for achieving holistic river management.

Appendix A: Verification of Simulation Results

The flow routing model used in this study was fully described in *Shiau and Wu* [2013], which was developed specifically for the planning and assessment purposes rather than the real-time optimal operation. The model built upon the established operation rules of the Feitsui Reservoir system and used the historical flow records (1998−2008) from two upstream tributaries as the input data to simulate the human-impacted flows at three connected reaches downstream of the reservoir. Several simplifications were adopted, including the unadapted water demands, unrestricted power generation, invariable reservoir capacity, and negligible runoffs generated downstream of the two gauging stations. The estimated initial and boundary conditions unavoidably introduced some uncertainties. In addition, the ad hoc emergency measures to cope with unexpected accidents or extreme events were not included in this generalized flow routing model.

The simulated and observed Q_A are given in Figures A1a and A1b, where reasonable agreement between the two series is shown. The ad hoc water-rationing measures taken in 2003 to cope with severe droughts were not fully reproduced. The model result exhibits a higher frequency of compelling releases, possibly due to the discrepancies in reservoir stages resulting from the supplemented hourly flow series and the adopted simplifications. To conduct a quantitative comparison, we show in Figure A1c the global wavelet power spectra (GWPS) of the simulated and observed results. Given the above-stated limitations, the two GWPS are in satisfactory agreement, where the global wavelet powers of the simulated result are almost consistently greater than those of the observed result at submonthly scales but reversed at scales longer than 1 month. Figure A1d reveals that the GWPS ratio has a maximum (=1.42) at subweekly scale and a minimum (=0.64) at annual scale, with an overall average of 1.03. Despite that the model result shows intensified flow oscillations at submonthly scales and attenuated ones at longer scales, our result indicates that these discrepancies are well below (less than 11%–52%) the human-induced flow regime alterations (see, e.g., Figure 6f).

Appendix B: Numerical Experiment of Regular Versus Random Releases

A numerical experiment was conducted using 4018 random numbers generated with a normal distribution whose mean and standard deviation are 10 and 1 m^3/s. This experiment is a reduced version of the release rules of the Feitsui Reservoir. The random numbers are taken as the daily 8 h release rates for a simulation period of 11 year (=4018 days), where these numbers are filled in two sets of hourly flow series that exhibit different release patterns. The first is a regular release pattern where each random number is taken as the daily release rate during 8 A.M. to 4 P.M.; the second is a random release pattern where a random number is taken to be the daily release rate during 12 P.M. to 8 P.M. if it is $\geq$ 10 m^3/s (=mean value), otherwise the random number is taken to be the daily release rate during 8 A.M. to 4 P.M., resulting in a 50% overall probability of delayed release. Shown in Figures B1a and B1b are sample hourly flow patterns (during the first week of year 1) of the regular and random releases, where an array of seven random numbers are assigned to the regularly and randomly spaced 8 h release intervals.

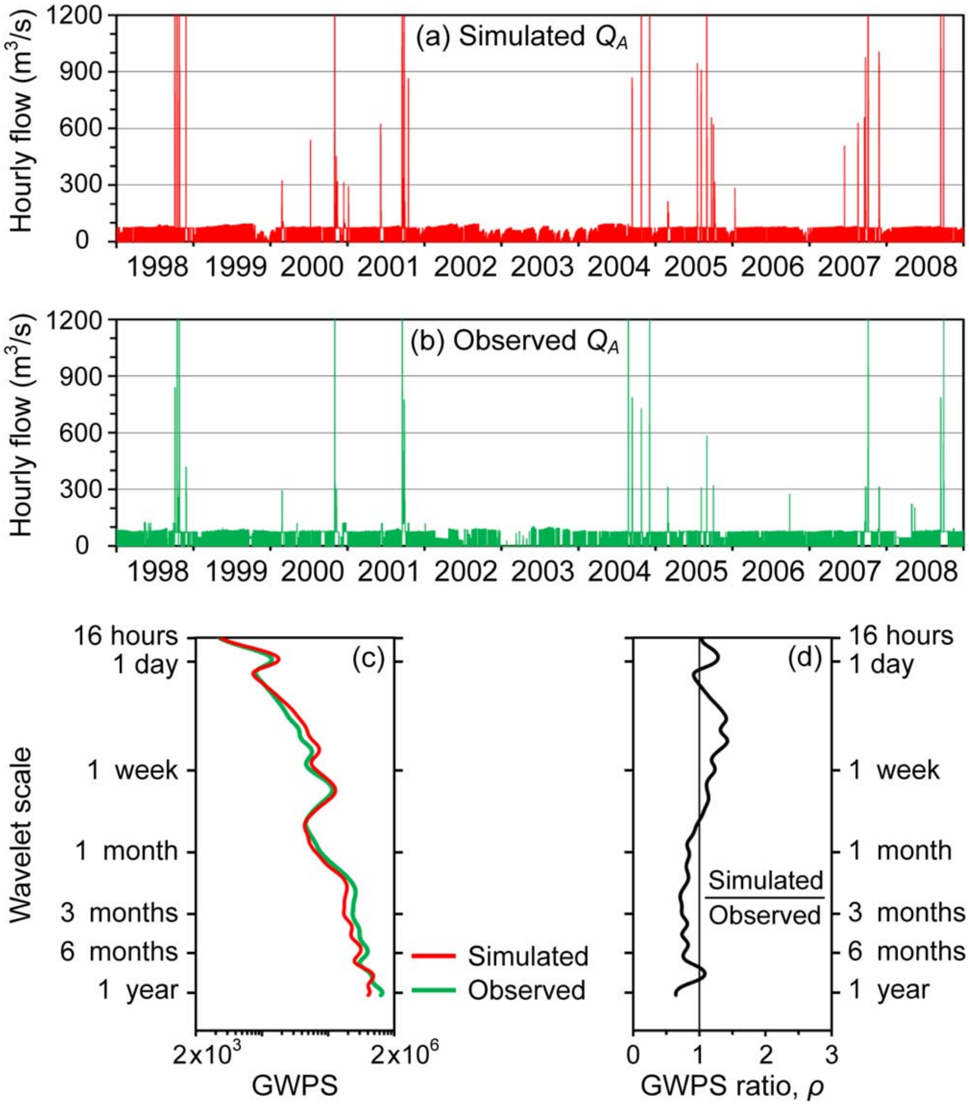

Figure A1. (a and b) Simulated and observed reservoir releases Q_A (truncated at 1200 m^3/s); (c) GWPS of simulated and observed Q_A; (d) GWPS ratio of simulated to observed Q_A.

The WPS diagrams corresponding to the regular and random releases over the 11 year simulation period are shown in Figures B1c and B1e, respectively. Figure B1c exhibits a clear-cut high-power (red) band at daily scale, accompanied by generally low wavelet powers at the remaining scales. The corresponding GWPS (Figure B1d) reveals that the global wavelet power at daily scale is 2 orders higher than those at the remaining scales, resulting in an abrupt drop of GWPS at 2 day scale. Figure B1e exhibits also a high-power band at daily scale, which is however followed by a smooth transition to the low power over submonthly scales, thus no abrupt drop of GWPS at 2 day scale is present in Figure B1f. These results demonstrate clearly the significant spectral differences between the strictly periodic daily release and cyclic (but not periodic) daily release even though they merely differ in the distribution of the 8 h release intervals (see Figures B1a and B1b). Such spectral differences are most notable at subweekly scales (see Figures B1d and B1f).

To quantitatively demonstrate the spectral differences between the two release patterns, we show in Figures B1g and B1h the GWPS ratio and GDWPS of the regular versus random releases. Figure B1g reveals that the most notable spectral differences are present at subweekly scales, where the GWPS ratios are consistently smaller than unity, with an extreme deviation from unity observed at 2 day scale. At daily scale the GWPS ratio is slightly greater than 1, while at scales longer than 1 month the ratios remain roughly as 1. Similarly, Figure B1h reveals that the most significant GDWPS are present at subweekly scales, with peak

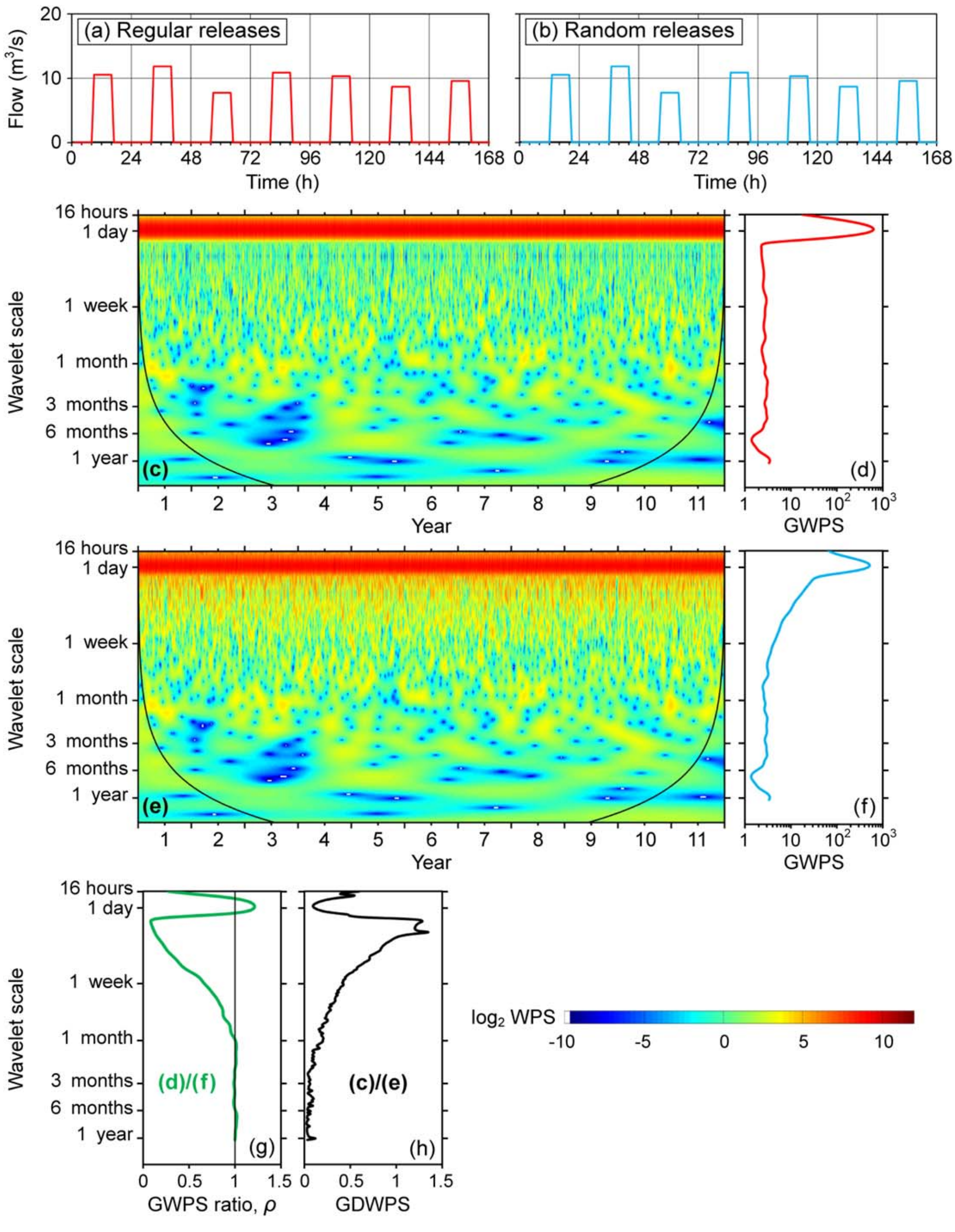

Figure B1. (a and b) Sample hourly flow patterns of regular and random releases (during the first week of year 1); (c and e) WPS diagrams of regular and random releases (year 1 to year 11); (d and f) GWPS of regular and random releases; (g and h) GWPS ratio and GDWPS of regular versus random releases. Base-2 logarithms of WPS are shown in Figures B1c and B1e in terms of color scale.

GDWPS observed at 2 day scale. The GDWPS at daily scale and scales longer than 1 month are close to 0. The GWPS ratio and GDWPS exhibit a common trend concerning the spectral differences between the regular and random release patterns.

In summary, this numerical experiment reveals that a set of flows released regularly with a 1 day period would result in a WPS that only exhibits high powers at daily scale, while the same set of flows released randomly with a 1 day cycle would result in a WPS exhibiting not only the high powers at daily scale but also significant powers at subweekly scales. The spectral differences between these two time series are most notable at subweekly scales, where the extreme GWPS ratio and peak GDWPS are both present at 2 days scale.

Notations

AWPS, SWPS	annually and seasonally averaged WPS.
CWT	continuous wavelet transform.
DFT	discrete Fourier transform.
DWPS	deviation between wavelet power spectra.
$DWPS_n(s)$	DWPS series.
GDWPS	globally averaged (or RMS) deviation between wavelet power spectra.
$GDWPS(s)$	GDWPS at scale s.
$GDWPS_{\text{sub}}(s)$	subflow GDWPS at scale s.
GWPS	global (or globally averaged) WPS.
$GWPS(s)$	GWPS at scale s, $GWPS1(s)$ and $GWPS2(s)=$ GWPS of $Q1_n$ and $Q2_n$.
$GWPS1_{\text{sub}}(s)$	GWPS of $Q1_{\text{sub},n}$.
IHA	indicators of hydrologic alteration.
N, n	length of time series, and time index.
Q_A, Q_B, Q_C	altered flow series at Reaches A, B, and C.
$Q_{A,\text{nat}}$	natural flow series at Reach A $(=Q_I)$.
$Q_{B,\text{nat}}$, $Q_{C,\text{nat}}$	natural flow series at Reaches B and C $(=Q_I+Q_N)$.
Q_{DV}	diversion rate at the Chingtan Weir.
Q_I, Q_N	reservoir inflows, and unregulated flows from the Nanshih Creek.
$Q1_n, Q2_n$	two flow series (not necessarily altered and natural series) to be compared.
$Q1_{\text{sub},n}$	subflow series of $Q1_n$.
R_D, R_{FL}, R_{HP}	release rates for domestic supply, flood control, and hydropower generation.
RMS	root-mean-square.
RVA	range of variability approach.
s, s_j	temporal scale (=period of wavelet oscillations).
s_0, s_J	shortest and longest scales.
TFRA, TPC	Taipei Feitsui Reservoir Administration, and Taiwan Power Company.
$W_n(s)$	CWT of time series at scale s, $\lvert W_n(s)\rvert=$ amplitude of $W_n(s)$.
WA	wavelet analysis.
WPS	wavelet power spectrum.
$WPS_n(s)$	WPS series $(=\lvert W_n(s)\rvert^2)$, $WPS1_n(s)$ and $WPS2_n(s)=$ WPS of $Q1_n$ and $Q2_n$.
$WPS1_{\text{sub},n}(s)$	WPS series of $Q1_{\text{sub},n}$.
x_n	discrete time series.
δs, δt	scale-sampling interval, and time interval for data sampling.
η	nondimensional time parameter.
$\rho(s), \rho_{\text{sub}}(s)$	GWPS ratio, and subflow GWPS ratio.
ω_0	dimensionless wave number.
Ψ, Ψ^*, Ψ_0	wavelet function, complex conjugate of Ψ, and mother wavelet function.

Acknowledgments
This study was supported by the Ministry of Science and Technology, Taiwan, with the research fund granted to F.C.W. (NSC 99–2221-E-002–172-MY3) and student award granted to C.F.C. (NSC 101–2815-C-002–111-E). TFRA and TPC are acknowledged for providing the flow records and reservoir operation data. These data are available upon e-mail request sent to the corresponding author. We are grateful to the thorough and insightful reviews offered by Stefano Basso, Andreas Efstratiadis, one anonymous referee, and Alberto Montanari, which helped improve this paper significantly.

References

Acreman, M. C., I. C. Overton, J. King, P. J. Wood, I. G. Cowx, M. J. Dunbar, E. Kendy, and W. J. Young (2014), The changing role of ecohydrological science in guiding environmental flows, *Hydrol. Sci. J.*, *59*, 433–450.

Adamowski, K., A. Prokoph, and J. Adamowski (2009), Development of a new method of wavelet aided trend detection and estimation, *Hydrol. Processes*, *23*, 2686–2696.

Arthington, A. H. (2012), *Environmental Flows: Saving Rivers in the Third Millennium*, Univ. of Calif. Press, Berkeley, Calif.

Arthington, A. H., and D. Sternberg (2012), Appendix 3: Freshwater fish-flow relationships and responses to flow regime alteration: A review of evidence from south-east Queensland streams, in *Hydro-Ecological Relationships and Thresholds to Inform Environmental Flow Management*, edited by A. H. Arthington et al., 24 pp., Int. Water Cent., Brisbane, Australia.

Baker, D. B., R. P. Richards, T. T. Loftus, and J. K. Kramer (2004), A new flashiness index: Characteristics and applications to midwestern rivers and streams, *J. Am. Water Res. Assoc.*, *40*, 503–522.

Bevelhimer, M. S., R. A. McManamay, and B. O'Connor (2015), Characterizing sub-daily flow regimes: Implications of hydrologic resolution on ecohydrology studies, *River Res. Appl.*, doi:10.1002/rra.2781, in press.

Botter, G., S. Basso, A. Porporato, I. Rodriguez-Iturbe, and A. Rinaldo (2010), Natural streamflow regime alterations: Damming of the Piave river basin (Italy), *Water Resour. Res.*, *46*, W06522, doi:10.1029/2009WR008523.

Bunn, S. E., and A. H. Arthington (2002), Basic principles and ecological consequences of altered flow regimes for aquatic biodiversity, *Environ. Manage.*, *30*, 492–507.

Deodhar, M. J. (2008), *Elementary Engineering Hydrology*, Pearson Educ., Delhi.

Farge, M. (1992), Wavelet transforms and their applications to turbulence, *Annu. Rev. Fluid Mech.*, *24*, 395–457.

Gao, Y., R. M. Vogel, C. N. Kroll, N. L. Poff, and J. D. Olden (2009), Development of representative indicators of hydrologic alteration, *J. Hydrol.*, *374*, 136–147.

Harman, C., and M. Stewardson (2005), Optimizing dam release rules to meet environmental flow targets, *River Res. Appl.*, *21*, 113–129.

Hughes, D. A., and S. J. L. Mallory (2008), Including environmental requirements as part of real-time water resources managements, *River Res. Appl.*, *24*, 852–861.

Instream Flow Council (2004), *Instream Flows for Riverine Resource Stewardship*, revised ed., Cheyenne, Wyo.

Jones, N. E. (2014), The dual nature of hydropeaking rivers: Is ecopeaking possible?, *River Res. Appl.*, *30*, 521–526.

Mathews, R., and B. D. Richter (2007), Application of the indicators of hydrologic alteration software in environmental flow setting, *J. Am. Water Resour. Assoc.*, *43*, 1400–1413.

Matos, J. P., T. Cohen, J.-L. Boillat, A. J. Schleiss, and M. M. Portela (2010), Analysis of flow regime changes due to operation of large reservoirs on the Zambezi River, in *Environmental Hydraulics*, edited by G. C. Christodoulou and A. I. Stamou, Taylor and Francis, London, U. K.

Meile, T., J. L. Boillat, and A. J. Schleiss (2011), Hydropeaking indicators for characterization of the Upper-Rhone River in Switzerland, *Aquat. Sci.*, *73*, 171–182.

Nakken, M. (1999), Wavelet analysis of rainfall-runoff variability isolating climatic from anthropogenic pattern, *Environ. Modell. Software*, *14*, 283–295.

National Research Council (NRC) (2007), *River Science at the U.S. Geological Survey*, Natl. Acad. Press, Washington, D. C.

Olden, J. D., and N. L. Poff (2003), Redundancy and the choice of hydrologic indices for characterizing streamflow regimes, *River Res. Appl.*, *19*, 101–121.

Percival, D. B., and A. Walden (2000), *Wavelet Methods for Time Series Analysis*, Cambridge Univ. Press, Cambridge, U. K.

Poff, N. L. (2009), Managing for variability to sustain freshwater ecosystems, *J. Water Resour. Plann. Manage.*, *135*, 1–4.

Poff, N. L., J. D. Allan, M. B. Bain, J. R. Karr, B. D. Prestegaard, B. D. Richter, R. E. Sparks, and J. C. Stromberg (1997), The natural flow regime: A paradigm for river conservation and restoration, *BioScience*, *47*, 769–784.

Richter, B. D., J. V. Baumgartner, J. Powell, and D. P. Braun (1996), A method for assessing hydrologic alteration within ecosystems, *Conserv. Biol.*, *10*, 1163–1174.

Richter, B. D., J. V. Baumgartner, R. Wigington, and D. P. Braun (1997), How much water does a river need, *Freshwater Biol.*, *37*, 231–249.

Shiau, J. T., and C. Y. Huang (2014), Detecting multi-purpose reservoir operation induced time-frequency alteration using wavelet transform, *Water Resour. Manage.*, *28*, 3577–3590.

Shiau, J. T., and F. C. Wu (2004a), Assessment of hydrologic alterations caused by Chi-Chi diversion weir in Chou-Shui Creek, Taiwan: Opportunities for restoring natural flow conditions, *River Res. Appl.*, *20*, 401–412.

Shiau, J. T., and F. C. Wu (2004b), Feasible diversion and instream flow release using range of variability approach, *J. Water Resour. Plann. Manage.*, *130*, 395–404.

Shiau, J. T., and F. C. Wu (2006), Compromise programming methodology for determining instream flow under multiobjective water allocation criteria, *J. Am. Water Resour. Assoc.*, *42*, 1179–1191.

Shiau, J. T., and F. C. Wu (2007a), A dynamic corridor-searching algorithm to seek time-varying instream flow releases for optimal weir operation: Comparing three indices of overall hydrologic alteration, *River Res. Appl.*, *23*, 35–53.

Shiau, J. T., and F. C. Wu (2007b), Pareto-optimal solutions for environmental flow schemes incorporating the intra-annual and interannual variability of the natural flow regime, *Water Resour. Res.*, *43*, W06433, doi:10.1029/2006WR005523.

Shiau, J. T., and F. C. Wu (2008), A histogram matching approach for assessment of flow regime alteration: Application to environmental flow optimization, *River Res. Appl.*, *24*, 914–928.

Shiau, J. T., and F. C. Wu (2009), Regionalization of natural flow regime: Application to environmental flow optimization at ungauged sites, *River Res. Appl.*, *25*, 1071–1089.

Shiau, J. T., and F. C. Wu (2010), A dual active-restrictive approach to incorporating environmental flow targets into existing reservoir operation rules, *Water Resour. Res.*, *46*, W08515, doi:10.1029/2009WR008765.

Shiau, J. T., and F. C. Wu (2013), Optimizing environmental flows for multiple reaches affected by a multipurpose reservoir system in Taiwan: Restoring natural flow regimes at multiple temporal scales, *Water Resour. Res.*, *49*, 1–20, doi:10.1029/2012WR012638.

Steel, E. A., and I. A. Lange (2007), Using wavelet analysis to detect changes in water temperature regimes at multiple scales: Effects of multi-purpose dams in the Willamette River basin, *River Res. Appl.*, *23*, 351–359.

Suen, J. P., and J. W. Eheart (2006), Reservoir management to balance ecosystem and human needs: Incorporating the paradigm of the ecological flow regime, *Water Resour. Res.*, *42*, W03417, doi:10.1029/2005WR004314.

Taipei Feitsui Reservoir Administration (TFRA) (2004), *Regulation Rules of the Feitsui Reservoir*, Taipei.

The Nature Conservancy (2009), *Indicators of Hydrologic Alteration Version 7.1 User's Manual*. Arlington, Va. [Available to https://www.conservationgateway.org/Files/Pages/indicators-hydrologic-altaspx47.aspx]

Torrence, C., and G. P. Compo (1998), A practical guide to wavelet analysis, *Bull. Am. Meteorol. Soc.*, *79*, 61–78.

Vogel, R., J. Sieber, S. Archfield, M. Smith, C. Apse, and A. Huber-Lee (2007), Relations among storage, yield and instream flow, *Water Resour. Res.*, *43*, W05403, doi:10.1029/2006WR005226.

White, M. A., J. C. Schmidt, and D. J. Topping (2005), Application of wavelet analysis for monitoring the hydrologic effects of dam operation: Glen Canyon Dam and the Colorado River at Lees Ferry, Arizona, *River Res. Appl.*, *21*, 551–565.

Yin, X. A., Z. F. Yang, and G. E. Petts (2011), Reservoir operating rules to sustain environmental flows in regulated rivers, *Water Resour. Res.*, *47*, W08509, doi:10.1029/2010WR009991.

Zimmerman, J. K. H., B. H. Letcher, K. H. Nislow, K. A. Lutz, and F. J. Magilligan (2010), Determining the effects of dams on subdaily variation in river flows at a whole-basin scale, *River Res. Appl.*, *26*, 1246–1260.

Zolezzi, G., A. Bellin, M. C. Bruno, B. Maiolini, and A. Siviglia (2009), Assessing hydrologic alterations at multiple temporal scales: Adige River, Italy, *Water Resour. Res.*, *45*, W12421, doi:10.1029/2008WR007266.

Zolezzi, G., A. Siviglia, M. Toffolon, and B. Maiolini (2011), Thermopeaking in alpine streams: Event characterization and time scales, *Ecohydrology*, *4*, 564–576.